

# Energy Advances

Accepted Manuscript

This article can be cited before page numbers have been issued, to do this please use: S. Mbatha, X. Cui, P. G. Panah, S. Thomas, K. Parkhomenko, A. Roger, B. Louis, R. Everson, P. Debiagi, N. Musyoka and H. W. Langmi, *Energy Adv.*, 2024, DOI: 10.1039/D4YA00433G.



This is an Accepted Manuscript, which has been through the Royal Society of Chemistry peer review process and has been accepted for publication.

Accepted Manuscripts are published online shortly after acceptance, before technical editing, formatting and proof reading. Using this free service, authors can make their results available to the community, in citable form, before we publish the edited article. We will replace this Accepted Manuscript with the edited and formatted Advance Article as soon as it is available.

You can find more information about Accepted Manuscripts in the [Information for Authors](#).

Please note that technical editing may introduce minor changes to the text and/or graphics, which may alter content. The journal's standard [Terms & Conditions](#) and the [Ethical guidelines](#) still apply. In no event shall the Royal Society of Chemistry be held responsible for any errors or omissions in this Accepted Manuscript or any consequences arising from the use of any information it contains.

# COMPARATIVE EVALUATION OF THE POWER-TO-METHANOL PROCESS CONFIGURATIONS AND ASSESSMENT OF PROCESS FLEXIBILITY

Siphesihle Mbatha<sup>a,c,\*</sup>, Xiaoti Cui<sup>e</sup>, Payam G. Panah<sup>e</sup>, Sébastien Thomas<sup>b</sup>, Ksenia Parkhomenko<sup>b</sup>, Anne-Cécile Roger<sup>b</sup>, Benoit Louis<sup>b</sup>, Ray Everson<sup>c</sup>, Paulo Debiagi<sup>f</sup>, Nicholas Musyoka<sup>f</sup>, Henrietta Langmi<sup>d</sup>

<sup>a</sup> HySA Infrastructure Centre of Competence, Centre for Nanostructures and Advanced Materials (CeNAM), Chemicals Cluster, Council for Scientific and Industrial Research (CSIR), Pretoria 0001, South Africa

<sup>b</sup> Institute of Chemistry and Processes for Energy, Environment and Health (ICPEES), UMR 7515 CNRS-University of Strasbourg, 25 rue Becquerel, Strasbourg 67087 Cedex 02, France

<sup>c</sup> Centre of Excellence in Carbon Based Fuels, School of Chemical and Minerals Engineering, Faculty of Engineering, North-West University, Private Bag X6001, Potchefstroom, 2531, South Africa

<sup>d</sup> Department of Chemistry, University of Pretoria, Private Bag X20, Hatfield, 0028, South Africa

<sup>e</sup> Department of Energy, Aalborg University, Pontoppidanstr. 111, 9220 Aalborg, Denmark

<sup>f</sup> Nottingham Ningbo China Beacons of Excellence Research and Innovation Institute, University of Nottingham Ningbo China, Ningbo 315100, PR China

\*Correspondence Emails: [siphe.mbatha94@gmail.com](mailto:siphe.mbatha94@gmail.com)

## ABSTRACT

This paper compares different power-to-methanol process configurations encompassing electrolyser, adiabatic reactor (s) and methanol purification configurations. Twelve different power-to-methanol configurations based on direct CO<sub>2</sub> hydrogenation with H<sub>2</sub> derived from H<sub>2</sub>O-electrolysis were modelled, compared, and analysed. High temperature solid oxide electrolyser is used for hydrogen production. Fixed bed reactor is used for methanol synthesis. The aim of the paper is to give detailed comparison of the process layouts under similar conditions and select the best performing process configuration considering the overall methanol production, carbon conversion, flexibility, and energy efficiency. ASPEN PLUS® V11 is used for flowsheet modelling and the system architectures considered are the open loop systems where methanol is produced at 100 kton/annum and sold to commercial wholesale market as the final purified commodity. Further optimization requirements are established as targets for future work. Three options of power-to-methanol configuration with methanol synthesis from CO<sub>2</sub> hydrogenation are proposed and further evaluated considering process flexibility. From the evaluation, the series-series based configuration with three adiabatic reactors in series performed better in most parameters including the flexible load dependent energy efficiency.

**Keywords:** Power-to-Methanol System Configurations, Process Design, Process Integration, Solid Oxide Electrolyser.



## 34 1. INTRODUCTION

35 Investment in renewable energy has been resilient to the Covid-19 pandemic.<sup>1</sup> With the ongoing transition  
36 to renewable energy sources particularly variable solar and wind, and the need for cleaner fuel derivatives,  
37 chemical energy storage stands central as the best potential solution to meet these sustainability goals.  
38 Methanol is a versatile chemical intermediate and due to its ease in handling, it is a robust renewable  
39 hydrogen carrier.<sup>2-6</sup> Recent study by Hank et al. investigated the potential to transport renewable hydrogen  
40 using methanol, ammonia, liquid organic hydrogen carriers and methane.<sup>3</sup> The study reiterated the  
41 significant potential of methanol to transport large amount of green hydrogen over long distances.<sup>3</sup> The fact  
42 that various value-added downstream chemicals can be produced from methanol (*i.e.*, the power-to-fuels),  
43 its ease in handling and the fact that it can be used directly in the fuel cells to produce electricity (*i.e.* the  
44 power-to-power architecture) makes it attractive.

45 Considering plant-to-planet analysis of green methanol via using planetary boundaries tool, González-  
46 Garay et al. discovered that the potential damage that green methanol can cause to the freshwater use,  
47 nitrogen and phosphorous flow are negligible when compared to the positive effects it will have on energy  
48 imbalances, CO<sub>2</sub> emission reduction and ocean acidification.<sup>7-8</sup> According to Moili et al. the hydrogen  
49 stored in methanol and methane processes are 85.3% and 78.2 %, respectively, thus indicating the good  
50 storage potential of methanol.<sup>4</sup> However, the methanol economy requires favourable policy directions.<sup>4-6</sup>  
51 In this front, majority of countries in the European Union (EU) as well as China have already announced  
52 ambitious plans to develop commercial scale renewable methanol plants by 2030.<sup>5</sup> Renewable Energy  
53 Directive II (RED II) of the EU requires that 14% of renewable energy derived fuels, including green  
54 methanol, be part of the transport sector by 2030.<sup>9</sup>

### 55 1.1 Recent progress in PtMeOH System level evaluation

56 Growing efforts are devoted to the so-called PtMeOH chain as a candidate process for sustainable methanol  
57 production via CO<sub>2</sub> valorisation and with hydrogen produced from renewable energy resources e.g. wind  
58 and solar via the electrolysis route.<sup>10-16</sup> Electrolysis technologies encompasses alkaline water-based  
59 electrolyser (AWE), polymer exchange membrane (PEM) and solid oxide electrolyzers (SOEC). Numerous  
60 studies have evaluated the energetic and techno-economic feasibility of PtMeOH.<sup>2-3, 17-24</sup> Rivera-Tinoco et  
61 al. deduced that SOEC-based PtMeOH has a higher energy efficiency (~54.8 %) than PEM-based  
62 PtMeOH.<sup>21</sup> Hank et al. evaluated the transport potential, techno-economics, and energy efficiency of PEM-  
63 based PtMeOH and deduced that the process has an energy efficiency in a range of 40–44% comparable to  
64 the power-to-methane process.<sup>3</sup> Zhang et al. evaluated the techno-economics of SOEC-based biomass-to-  
65 methanol process and deduced that an energy efficiency of 66 % can be achieved from this process and  
66 highlighted a trade-off between the system efficiency and its production cost.<sup>22</sup> However, biomass-based



67 processes are limited by biomass feedstock availability.<sup>20</sup> Zhang et al. investigated the techno-economic  
68 optimization of the SOEC-based PtMeOH process and similarly observed that there is a trade-off between  
69 the energy efficiency and the production costs.<sup>22</sup> Bos et al. investigated the techno-economics of a 100 MW  
70 wind-based PtMeOH plant with hydrogen produced from AWE and concluded that the process has an  
71 energy efficiency of 50%.<sup>17</sup> Al-Kalbani et al. compared the environmental performance of fossil fuel-based  
72 and renewable energy-based PtMeOH, and their findings depicted that renewable energy-based PtMeOH  
73 is attractive from an environmental perspective.<sup>18</sup> The main conclusion from these studies points to high  
74 energy demands and high hydrogen production and electrolyser capital costs as the major techno-economic  
75 feasibility barriers.<sup>3</sup> The availability of power determines the quantity of hydrogen that can be produced  
76 and therefore the optimal capacity and system configuration.<sup>7,17</sup> It also emanates from these studies that the  
77 SOEC is an attractive technology from the perspective of energy efficiency and for coupling with  
78 exothermic processes such as methanol production process, although further improvements on the SOEC  
79 technology (e.g. flexibility) is still required to make its application in renewable PtMeOH more competitive.

80 On the other hand, these studies highlighted the required improvements in carbon capture technologies,  
81 particularly from the confines of energy penalty and costs reduction.<sup>7,17</sup> According to Bos et al., the  
82 methanol synthesis loop is dominated by feed compression and the key to optimizing the costs and  
83 productivity is to find the favourable ratio between the reactor size(s) and compression requirements such  
84 that the reactor operation pressure and cost of compressors remains optimized.<sup>9, 17</sup> The latter approach is  
85 limited by the trade-offs between pressure (i.e. feed compression duties) and conversion due to  
86 equilibrium.<sup>7</sup> An alternative is to reduce the recycle compression by increasing the single pass conversion,  
87 but according to González-Garay et al. and Alsuhaibani et al. this strategy has limited impact on profitability  
88 relative to decreasing the overall reactor pressure.<sup>7, 23</sup> Thus efforts in finding cheap and easy to scale  
89 catalysts that operates efficiently at lower pressures (<50 bar) shall not cease and their effects will become  
90 more dominant (~24.4% share of the total costs) when power-to-methanol is already economically feasible.<sup>7</sup>  
91 Furthermore, a combination of economically effective yield and pressure needs to be identified.<sup>7</sup>

92 It is also evident from the highlighted studies that, recently, the system level optimization has emerged as  
93 a new paradigm shift needed to improve the economics of the process.<sup>24-29</sup> To accelerate technology  
94 readiness and techno-economic improvement of PtMeOH, several demonstration projects have been  
95 implemented and some are being planned.<sup>26</sup> Nonetheless, availability of data from demonstrated systems  
96 remains scarce and difficult to access. On the other hand, modelling efforts in this direction have thus far  
97 been directed to a single objective or only two objectives i.e. energy efficiency and production costs. Thus,  
98 optimized process flowsheets that enhances the CO<sub>2</sub> and H<sub>2</sub> conversions, energy efficiency, process  
99 economic (lowering production costs and/or capital), flexibility and reduce CO<sub>2</sub> emissions and system



100 complexity are required.<sup>3</sup> Due to low conversion of the direct CO<sub>2</sub> hydrogenation over the Cu/ZnO/Al<sub>2</sub>O<sub>3</sub>,  
101 GhasemiKafrudi et al. optimised the process recycle flow to improve the performance.<sup>24</sup> They considered  
102 different process parameters, including temperature, pressure, and GHSV, to reduce the recycle, energy  
103 consumption and greenhouse gas emissions of the CO<sub>2</sub> hydrogenation process. Furthermore,  
104 GhasemiKafrudi et al., investigated the effect of changes in the hydrogen injection as make up gas, applying  
105 two reactors, inert gases, moisture in the feed, the use of dry hydrogen and the recycle stream on methanol  
106 yield.<sup>24</sup> Their results showed that having two reactors with intermediate dehumidification in series and  
107 adding hydrogen as make-up at the inlet of the second reactor increases the methanol yield by a factor of  
108 1.8.<sup>27</sup> However, the authors also deduced that if one reactor with recycle is used, the resultant methanol  
109 yield is almost double when compared to the case of one reactor with no recycle.<sup>24</sup> Finally, GhasemiKafrudi  
110 et al., concluded that by just modifying the catalyst type and total amount (decrease slightly e.g. in their  
111 case; total amount =865kg) and increasing the inlet temperature (e.g. in their case to 209 °C), the recycle  
112 flow reduces by almost 38%.<sup>24</sup> Moioli et al. and Lee et al. have already established that for a CO<sub>2</sub>  
113 hydrogenation on Cu/ZnO/Al<sub>2</sub>O<sub>3</sub> based catalyst, and for both small scale and commercial scale (~100  
114 kton/annum), three cascade fixed-bed reactors are optimal.<sup>4,14</sup> Lee et al. deduced that a configuration with  
115 three reactors in series, having intermediate cooling and separation of methanol/H<sub>2</sub>O between the reactors  
116 is optimal in-terms of profit (from a deficit of \$4.3 to \$2.5 profit per ton) and CO<sub>2</sub> conversion (~52%).<sup>14</sup>  
117 However, Lee et al. using a process superstructure and techno-economic optimization methods investigated  
118 the best configuration that optimizes the profit for the two step CO<sub>2</sub> hydrogenation process in which both  
119 CO<sub>2</sub> and CO participate as carbon sources in hydrogenation reactions to methanol and focusing only on the  
120 synthesis and purification step instead of the direct CO<sub>2</sub> hydrogenation process as will be considered in this  
121 study.<sup>14</sup> Furthermore, the superstructure optimisation approach tends to discard the suboptimal flowsheets  
122 following set objectives and constraints without giving further details as to why the suboptimal process  
123 underperforms and the possibility of improving it further.<sup>27</sup>

124 More recently, Chiou et al. investigated six different configurations for the PtMeOH focusing on single  
125 stage and multistage series reactor(s) connections with adiabatic and non-adiabatic (with co-current  
126 cooling) reactor type.<sup>28</sup> Their study focused on design, optimisation, control, techno-economics, and  
127 environmental aspects of the process considering a small scale (20 kton/y) plant capacity. They reached the  
128 conclusion that two reactors with first stage non-adiabatic (with co-current cooling) and second stage  
129 adiabatic reactor type in series with inter-stage cooling and separation of methanol and water was more  
130 economically attractive (with a minimum selling price of methanol of 998US\$/ton and carbon tax of  
131 283US\$/ton) and showed better performance. From this, they devised a control strategy aimed at handling  
132 the throughput and compositional disturbances for their proposed configuration. The rejection of two kinds  
133 of compositional disturbances i.e. (i) the 5% N<sub>2</sub> and (ii) the H<sub>2</sub> impurity were investigated. Their control



134 strategy allowed the rejection of both compositional disturbances within 5h. It was noted that increases in  
135 N<sub>2</sub> impurity composition deteriorates the reaction kinetics and increases the purge rate which reduces  
136 methanol production rate with higher loss of CO<sub>2</sub> and H<sub>2</sub>. Thus, to maintain the single pass conversion, H/C  
137 ratio will have to be increased. The authors however did not investigate any full integrated process with  
138 electrolyser, parallel-series configuration, and the three-stage reactors with intercooling, nor the detailed  
139 load change flexibility of their system.

## 140 **1.2. Recent progress in PtMeOH process flexibility**

141 Production processes are prone to stochastic variation for example in system input parameters, internal  
142 process parameters and environmental factors.<sup>30</sup> A degree of process flexibility helps to deal with these  
143 challenges. The level of process flexibility affects the economic gain of the process and the selection of the  
144 right conditions (i.e. parameters, location, capacity, etc.) in which the process operates economically.<sup>30-33</sup>  
145 In this paper, flexibility refers to the ability to handle the changes in the feedstock composition/flow or  
146 adjustments to other changing boundary conditions in order to adapt the plant operation to the changes in  
147 the energy or material supply.<sup>34</sup> It is well-known that the electrolyser, in particular the PEM type which is  
148 suitable for rapid start-up, can provide good flexibility.<sup>32,35-36</sup> Lange et al. recently gave a good technical  
149 review of the state of the art of the electrolyser technology's flexibility including the SOEC technology  
150 which will be considered in this study due to its high efficiency.<sup>36</sup> Lange et al. deduced that the SOEC can  
151 provide a broad range of load flexibility (-100% to 100 %), but this is countered by its long cold-startup  
152 time (~60min).<sup>36</sup> However, efforts are being made on the front of improving the performance of the  
153 materials for the SOEC cells/stack to allow more flexibility and shorten the start-up time without incurring  
154 severe cell damage.<sup>36-37</sup> The recent results such as in the work of Li et al. showed great potential of the  
155 future of the SOEC in handling flexibly the intermittent renewable energy supply with reduced start-up  
156 time.<sup>37</sup>

157 In a coupled electrolysis-methanol synthesis system, intermediate gas (hydrogen and CO<sub>2</sub>) storage under  
158 intermittent conditions may be needed unless the reactor operates flexible. If the reactor has a wide tolerance  
159 to variations in the operational parameters, it is referred to as the load flexible reactor. The load range of  
160 the catalytic reactor is a function of chemical reactions, transport rate, catalysts, and reactor design.<sup>32</sup> The  
161 attainable load flexibility of the methanol reactor section has not been investigated, at-least intensively.<sup>31-</sup>  
162 <sup>33</sup> At the present, to the author's knowledge, only INERATEC GmbH has expressed interest to investigate  
163 and scale-up the flexible modular micro-structured reactors. Considering the case of variable renewable  
164 energy-based processes, flexibility is typically achieved by over-sizing the main process equipment to  
165 account for variability in the load. The size of the equipment directly influences the propagation of  
166 disturbances within the unit and the bigger the size, the smaller the influence of disturbances on process





167 variables. However, the load range of the reactor is also limited by operational issues such as maximum  
168 temperature rise and ability to achieve autothermic control i.e. in which the reactor outlet is used to heat the  
169 feed (via feed-effluent heat exchanger concept).<sup>31</sup> The heat of reaction is, with careful heat management,  
170 generally enough to heat the feed to the methanol synthesis reactor(s) and/or distillation column, thus  
171 allowing the system to operate autothermally i.e. achieving energy self-sufficiency without external  
172 heating/cooling. In cases where the reactor feed stream is not sufficiently heated, the reaction rate will  
173 decrease and thus rendering low outlet temperature, which in effect results into lower inlet temperature and  
174 consequently the reaction halts completely. According to the study on fixed bed reactors performed by  
175 Zimmermann et al., with methane as an example, the step responses typically implemented by switching  
176 from one steady-state to another were found to be the worst-case load change policy due to the existence  
177 of unfavourable behaviour such as temperature overshoot and conversion drops.<sup>38</sup> Proper design of the  
178 network structure can help achieve necessary flexibility without additional oversizing of the equipment.<sup>39</sup>  
179 According to Grossmann & Morari, flexibility cannot be simply achieved by ad hoc addition of equipment  
180 or oversizing but by systematic design techniques.<sup>40</sup>

181 Rinaldi & Visconti assessed the steady state and transient performances of a multi-tubular fixed bed reactor  
182 for methanol production from biogas.<sup>41</sup> Their modelled system had a methanol synthesis reactor, a flash  
183 unit, and accounted for the unconverted gas recycle. The novelty of their conceptual work was to assess the  
184 possibility to run a multi-tubular methanol synthesis reactor flexibly, i.e., using the carbon dioxide from  
185 biogas and renewable H<sub>2</sub> in order to increase methanol productivity when the process is economically  
186 feasible. In their work, the investigation of the methanol synthesis multi-tubular reactor is conducted  
187 considering the impacts, on methanol productivity, temperature profile and transient behavior, of the two  
188 operating conditions i.e. (i) when the cost of green hydrogen is high, the excess of CO<sub>2</sub> in the biogas is  
189 vented and the reactor is fed with CO<sub>2</sub>-lean syngas only; (ii) conversely, when affordable renewable H<sub>2</sub> is  
190 available, CO<sub>2</sub> is co-fed into the reactor along with this affordable green H<sub>2</sub>.<sup>41</sup> These authors compared a  
191 1D and 2D model in terms of its ability to better predict the temperature and production profile.<sup>41</sup> They  
192 deduced that the concerned reactor manages well both operating conditions with steady state reached within  
193 a few hours when switching from one condition to another and that 2D model are better suited to predict  
194 the temperature and methanol production profile. Moreover, they also highlighted that reducing the number  
195 of tubes (equivalent to the reducing catalyst amount and measured using GHSV) instead of the reactor  
196 length is preferred especially for small scale processes. Reducing the length of the reactor can lead to  
197 unacceptable hot-spots from the resultant worsening of the convective heat transfer and reduced selectivity  
198 to methanol. When the length of the reactor is shortened, the thermal peak is achieved at higher  
199 temperatures, and the gaseous stream remains mostly in the kinetic regime to near the end of the reactor.<sup>41</sup>



200 This was prevalent when syngas is fed with and without co-feeding the CO<sub>2</sub> and H<sub>2</sub>, and when the length  
201 of the reactor was decreased below half (up to ¼ ) of the original length.<sup>41</sup>

202 Furthermore, Svitnič and Sundmacher investigated the effect of flexibility of the methanol synthesis process  
203 on the levelized cost of methanol (LCOM).<sup>42</sup> In their finding, the flexibility gains are most prominent for  
204 the designs with a single source of renewable energy (either solar or wind) leading to reduction of costs of  
205 more than 10%. This gain is significantly reduced for the design with combined solar and wind resources,  
206 as the complementary availability of renewable resources allows to better sustain stable operation of the  
207 chemical processes, reducing the influence of flexibility to 5.1%. Moreover, the authors deduced that the  
208 flexible operation of the methanol synthesis has a stronger effect on the reduction of LCOM, where for the  
209 design with a single renewable resource it delivers a roughly 4-times larger reduction of LCOM.

210 More recently, Qi et al. investigated different strategies for flexible operation of the power-to-X processes  
211 coupled with renewables using PtMeOH as a reference.<sup>33</sup> The strategies they compared involved the use of  
212 the energy buffers i.e. the hydrogen intermediate storage, liquid CO<sub>2</sub> energy storage as a Carnot battery,  
213 and Li-ion battery storages. In considering the latter they generated nine process configurations with  
214 islanded, grid-assisted only, and grid-assisted bidirectional connections for allocation of energy. Qi et al.  
215 considered a combination of solar and wind energy as well as grid electricity purchase.<sup>33</sup> The configurations  
216 with grid-assisted bidirectional connections resulted into the most cost-effective way for flexible operation  
217 of the power-to-X and the lowest levelized cost (~479.4 US\$/ton) was achieved when the Carnot battery  
218 was used. However, this is still more expensive than the methanol produced from autothermal reforming of  
219 natural gas which can reach a cost of 285.6US\$/ton and thus indicating that further research and  
220 development is needed to make renewable methanol production cost-competitive with other methods. In  
221 addition, some trade-offs were observed amongst the performance indexes which indicate that there is no  
222 single best solution but rather more case dependent solutions. Moreover, studies are required that  
223 incorporate the dynamic modelling of the energy buffer and the electrolyser to account for the factors such  
224 as the time varying energy efficiency and the limitations on power ramp-up.<sup>33</sup> Process operation can  
225 influence the design of the process and hence the flowsheet. Compared to investigations focusing on  
226 methanol synthesis catalyst improvements, studies focusing on PtMeOH reactor design, process  
227 configurations and process flexibility are very few. The objective of this paper is to model and compare  
228 different PtMeOH process layouts under steady state and dynamic conditions with the consideration of their  
229 process flexibilities.

### 230 1.3 Statement of originality

231 The originality of the work in this paper lies in the comparative flexibility analysis of different integrated  
232 methanol synthesis system configurations comprising parallel-series and series-series connections. Twelve





233 integrated flowsheets (including co-electrolysis and the electrified reverse water gas shift (e-RWGS)  
234 system) based on SOEC, methanol synthesis and purification steps are contrasted to assess their  
235 performance in terms of energy efficiency, production rate, and material conversion. In addition, the better  
236 performing CO<sub>2</sub> hydrogenation-based flowsheets are assessed under dynamic mode for their flexibility and  
237 to answer the following questions:

- 238 1) What is the feasible (with minimum sophisticated equipment) load-change flexibility window?
- 239 2) What is the effect of the load change in the parallel-series and series-series-based configurations?
- 240 3) How do the energy efficiency and conversion in the mentioned flowsheets design changes with the  
241 change in the load?

242 Candidate PtMeOH configuration(s) with methanol synthesis from CO<sub>2</sub> hydrogenation is proposed.  
243 Furthermore, optimization requirements are established as targets for future work. The paper is structured  
244 as follows: Section 2 gives the base content and approach to modelling, Section 3 gives the detailed results  
245 and discussion, Section 4 concludes the work and Section 5 give recommendations for future work.

## 246 2. PROCESS SYNTHESIS AND MODELLING

247 Twelve different flowsheets are synthesized and simulated (see section 2.2.2 table 6 and supplementary  
248 material section A2 for more details) under steady state conditions in Aspen Plus® V11 and out of the  
249 twelve, three are selected for flexibility assessment under Aspen Dynamics V11 platform. Table 1 shows  
250 the assumptions pertaining feed conditions. The system's capacity is designed to store about 162 MW of  
251 renewable electricity from either wind or Solar PV farm. This is in scale of a commercial size plant.<sup>43-45</sup> For  
252 all flowsheets, the SOEC configuration was left unchanged, however the methanol synthesis section  
253 configuration was modified to generate twelve different process configurations. Following the findings of  
254 Samimi et al. on the possibility to enhance the production rate of methanol with exclusion of inert in the  
255 feed, inert are thus neglected in this study.<sup>46</sup>

256 Table 1: Feed conditions.

Raw materials	Temperature(°C)	Pressure (bar)	Flowrate (kmol/hr)	Composition (mol %)
CO <sub>2</sub>	25	1.0	401	100
H <sub>2</sub> O	25	1.0	1232	100
Sweep gas (oxygen)	25	1.0	31	100
<b>Steam electrolysis product H<sub>2</sub> feed stream to MEOH unit</b>				
H <sub>2</sub>	35	5.0	1212.5	98.8
H <sub>2</sub> O	35	5.0	14.3	1.2
<b>Co-electrolysis product syngas feed stream to MeOH unit</b>				
H <sub>2</sub>	35	5.0	1212.5	74.3
CO <sub>2</sub>	35	5.0	105	6.4
CO	35	5.0	296	18.1
H <sub>2</sub> O	35	5.0	19.3	1.2

257



258 The exclusion of inert allows setting the lowest possible purge as detected by the system control  
259 parameters.<sup>9, 47</sup> Recycle ratio is an effective control parameter of the process (particularly the reactor)  
260 productivity and temperature.<sup>46</sup> It is also critical to highlight that the dynamic modelling of the SOEC to  
261 ascertain its capability is beyond the scope of this work. Rather the focus on dynamic modelling is placed  
262 on the downstream reactor configurations to establish their flexibility.

## 263 2.1 SOEC modelling

264 The electrochemical model to simulate the SOEC was implemented in ASPEN PLUS® V11 in the  
265 FORTRAN routine with the use of design specifications and calculator functions. Water, sweep-gas  
266 (oxygen) and electricity are the primary feeds to the SOEC unit. The thermodynamic model used in  
267 modelling the electrolysis is the Redlich-Kwong Soave equation of state (EOS) with modified Huron-Vidal  
268 mixing rules (RKSMHV2).<sup>48-50</sup> The main electrochemical model is a function of product species, which are  
269 electrochemically active i.e.  $i=H_2$ . The net voltage is expressed by equation 1 below:

$$270 \quad E_i = E_{nerst,i} + E_{act,i}^{her} + E_{act,i}^{oer} + E_{ohm,i} + E_{mic,i} \quad (1)$$

271 Where  $E_{nerst,i}$  is the Nernst potential,  $E_{act,i}$  refers to the over-potential due to activation of electrochemical  
272 reactions,  $E_{ohm,i}$  refers to the ohmic over-potential and  $E_{mic,i}$  is the interconnect voltage losses. The  
273 system is assumed to operate at thermoneutral stack voltage and under steady state, thus equation 2 is used  
274 as the main equation to calculate the thermoneutral energy.

$$275 \quad E_{tn} = \frac{\Delta H_r}{I_{tot}} = E_i \quad (2)$$

276 Where  $\Delta H_r$  is the heat of reaction, and  $I_{tot}$  refers to the total current (A). According to Giannoulidis et al.  
277 it is advantageous from the perspective of the SOEC energy efficiency to operate the unit at low pressure  
278 (<10 bar).<sup>2</sup> For the selected operating conditions, thermoneutral operation is achievable.<sup>45, 51</sup> Generally, the  
279 planar O-SOEC is operated in the temperature range of 150 °C – 950 °C and pressure range of 1–8 bar.<sup>2,52–53</sup>  
280 The SOEC operating under co-electrolysis conditions can already produce syngas at ratio of 1.5 to 3.5.<sup>53</sup>  
281 The SOEC unit capacity is designed for 109 MW considering the SOEC operating under steam electrolysis  
282 only. However, for the co-electrolysis based SOEC unit capacity only 134 MW is required to produce the  
283 syngas given in Table 2. Table 2 shows the input parameters used in the modelling of the SOEC unit.  
284 Generally operating the SOEC at higher temperature lowers the electricity requirements and hence increases  
285 the energy efficiency. The choice of temperature is a reasonable compromise between allowable  
286 concentration over-potential, ohmic over-potential and possibility of achieving thermo-neutral point  
287 operation.

288



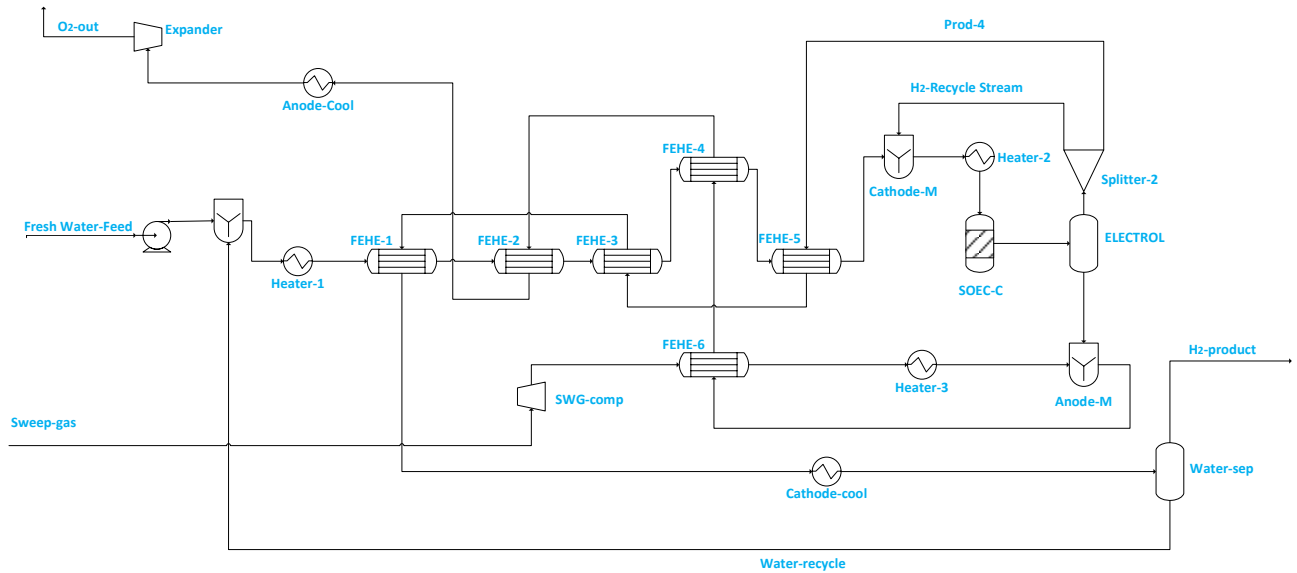
289 Table 2: SOEC operating conditions and parameters for steam and co-electrolysis

Parameter	Value	Unit
Steam inlet temperature of SOEC	850	°C
Air inlet temperature of the SOEC reactor	850	°C
SOEC stack temperature	850	°C
Reactant utilization	70	%
H <sub>2</sub> cathode inlet recycle	10	%
Operation pressure	5.0	bar
Stack consumption	29.7	kWh/kgH <sub>2</sub>
Hydrogen production	2827	kg/h
Syngas production	15360	kg/h
Syngas ratio (methanol feed)	2.2	-
LHV of syngas	25	MJ/kg

290

291 Typically, near or at thermoneutral point, high electrolysis efficiency and minimum sweep gas flowrate are  
 292 achievable.<sup>2</sup> This makes operating the electrolyser at thermoneutral point attractive.<sup>2,54–55</sup> Figure 1 illustrates  
 293 the SOEC model flowsheet for steam electrolysis implemented in ASPEN PLUS. Figure 2 illustrates the  
 294 SOEC model flowsheet for co-electrolysis implemented in ASPEN PLUS. For steam electrolysis (see  
 295 Figure 1), demineralized water (stream WATER) is first pumped to increase its pressure to SOEC operating  
 296 pressure, then vaporised and superheated in a cascade of heat exchangers, and mixed (via CATHOD-M)  
 297 with cathode feed recirculation (i.e. stream H<sub>2</sub>-Recycle stream) which contains 10 mol% of hydrogen.<sup>56–60</sup>  
 298 The fraction hydrogen is recycled to prevent electrode (i.e. Ni-YSZ) re-oxidation.<sup>56</sup> The composition of  
 299 steam in the SOEC feed (i.e. stream SOEC-FEE) is maintained above 90% to prevent starvation at the  
 300 electrode, which may cause cell damages. The SOEC cathode is modelled using RSTOIC, using the  
 301 conditions in Table 2 and the feed steam utilization factor (i.e. in the SOEC-C unit) is assumed to be 70%.  
 302 The product stream (i.e. stream PRODUCT-1) containing oxygen, hydrogen and unconverted water of the  
 303 SOEC cathode (SOEC-C) is separated in the electrolyte (i.e. ELECTROL) into PRODUCT-2 and  
 304 PRODUCT-3. Stream PRODUCT-3 contains only water and hydrogen, and it is split (i.e. SPLIT) into  
 305 product stream containing wet hydrogen (i.e. stream PROD-4) and recycle stream (i.e. H<sub>2</sub>-RECYC). Stream  
 306 PROD-4 is used to pre-heat the feed stream, and it is ultimately cooled and fed to the separator block (i.e.  
 307 WATER-SEP) in which a significant quantity of water (i.e. stream WWATER) is removed (discharged or  
 308 recycled) and wet hydrogen at 98.8 mol% is fed to the methanol synthesis section. Stream PRODUCT-2  
 309 contains only oxygen. The cascade heat exchanger network is used to recuperate the heat from the effluent  
 310 streams for the purpose of generating superheated steam at cheaper cost. Sweep gas (i.e. stream SWEEP-  
 311 GA) is assumed to contain only oxygen and is first compressed (via COMP-1) to SOEC pressure, heated  
 312 (via FEHE 2, HEATER 2) to SOEC temperature and fed to anode side (i.e. modelled as ANODE-M) of the  
 313 SOEC unit to remove the oxygen produced during electrolysis. The removed oxygen is then used in the  
 314 cascade heat exchangers to preheat steam, after which it is then cooled and expanded to atmospheric  
 315 conditions before being discharged or alternatively sold or sent to another process (i.e. stream O2-DISCH).

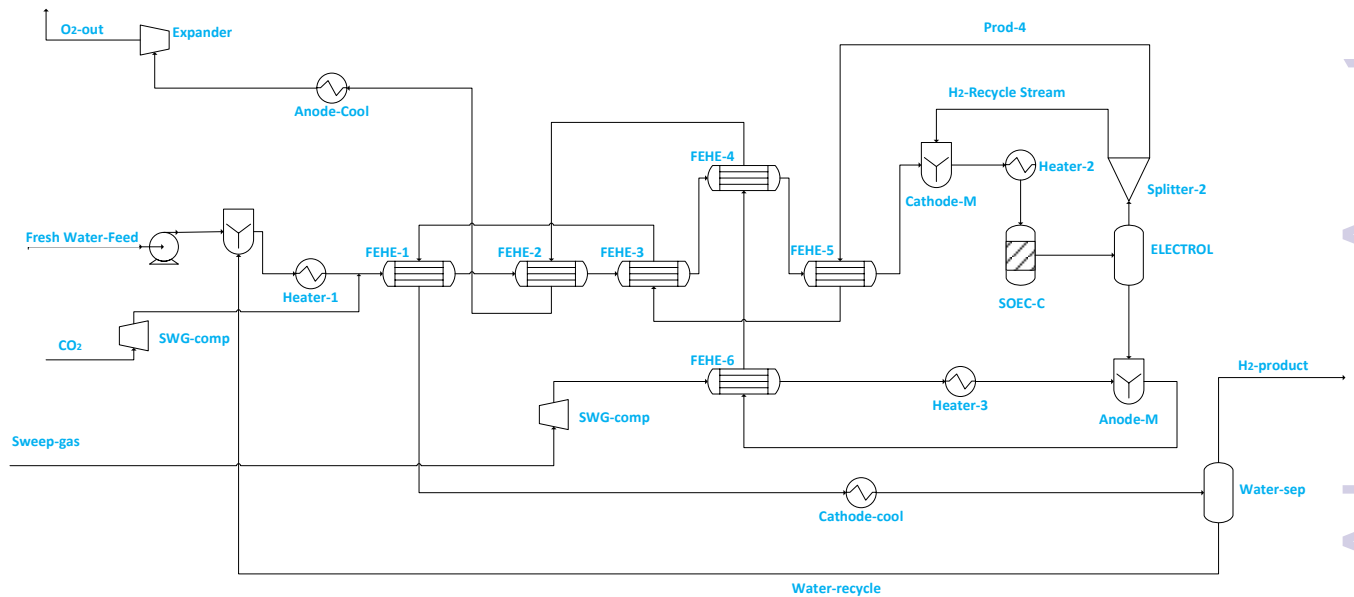




316

317

Figure 1 Illustration of the SOEC unit used for steam electrolysis in ASPEN PLUS®.



318

319

Figure 2 Illustration of the SOEC unit used for co-electrolysis in ASPEN PLUS®.

320 The use of oxygen (recirculated) as a sweep gas manages possible overshoot in the over-potential; therefore  
 321 allows for higher energy efficiency operation of the electrolyser. During the start of the process, oxygen is  
 322 assumed to come from its storage tank, while during operation it can be recirculated from the anode with  
 323 some stored or sold to end users. It is noted beforehand that the use of oxygen may increase the exergy  
 324 destruction, but the difference between the exergy efficiency when steam or air is used as sweep gas is  
 325 expected to be marginal, with steam as sweep gas having the exergy efficiency which is ~1% more than  
 326 that of oxygen.<sup>47,57</sup> In addition, using oxygen as a sweep gas allows the production of pure oxygen which  
 327 can be sold to market.<sup>47, 57</sup>



## 2.2 Steady state: reactors and separation modelling

Both CO<sub>2</sub> and H<sub>2</sub> feed streams are compressed to 78 bar using multiple compressors each with an isentropic efficiency of 75% for the steam electrolysis-based PtMeOH. For the co-electrolysis-based system, the syngas feed is compressed in a two-stage compression system to 78 bar with same isentropic efficiency. Considering safety aspects as it would be necessary in real plants, the compression ratio is kept at 3 and inter-stage cooling is included. The temperature of the feed stream to reactor(s) was set to 210 °C.<sup>61</sup> The inlet temperature is in a typical range of an optimised industrial methanol reactor<sup>61</sup>, a higher inlet temperature can result in a higher outlet temperature and a lower methanol yield, particularly for the adiabatic reactor(s). In addition, the lower limit for allowable inlet temperature is defined by the catalyst, and for the commercial copper-based catalyst it is around 190 °C.<sup>62</sup> Commercial Cu/ZnO/Al<sub>2</sub>O<sub>3</sub> catalyst is used in this study. Reactor (s) is modelled as an adiabatic reactor(s). Table 3 gives the properties of adiabatic reactor(s) modelled as a plug-flow (RPLUG) and those related to the catalyst. Adiabatic reactors have lower cost relative to the water-cooled and gas-cooled reactors due to their simple structural designs.<sup>62</sup> The advantage of adiabatic reactors is that under nominal steady state conditions their size is very small, thus their over-sizing slightly affect the capital cost.<sup>63-65</sup> This indicates their potential in small scale PtMeOH processes as well.<sup>62</sup> The reactor size was selected to be large enough such that the effluent from the reactor is near equilibrium.<sup>47</sup> Redlich-Kwong-Soave equation of state with modified Huron-Vidal mixing rules (RKSMHV2) was used to model the reactor(s), auxiliaries and to calculate the thermodynamic properties of the streams (refer to Section A1 of the Supplementary Material). After separation of methanol and water using a flash drum, a recycle stream was then purged up to 0.1% for all flowsheets (see section A4.2 of the supplementary material for the sensitivity on recycle fraction). In line with the work of Cui *et al.*, the small purge of 0.1% was set, which aims to minimize the CO<sub>2</sub> emission for the green methanol production.<sup>66</sup> As observed from Cui *et al.* using a larger purge ratio can result in lower flow rate of the recycle stream as well as a smaller reactor size but a higher CO<sub>2</sub> loss. It was also observed from Cui *et al.* that a value lower than 0.1% may cause convergence problem.<sup>66</sup> For the syngas (co-electrolysis-based system), the purge stream after methanol separation and recycle was set to 1.3%.

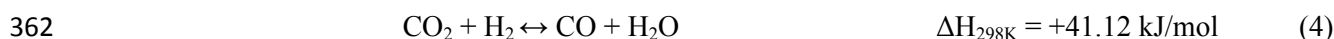
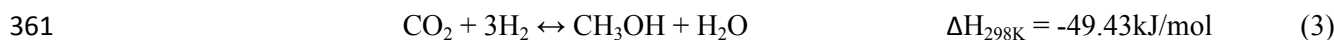
Table 3: Adiabatic plug-flow reactor (s) operating conditions

Parameter	Value	Unit
Tube diameter	3-5	m
Tube length	3-12	m
Reactor inlet pressure	74-75.7	bar
Catalyst particle density	1775	kg/m <sup>3</sup>
Bed porosity	0.5	-
GHSV	4000-7300	h <sup>-1</sup>



### 355 2.2.1. Reaction kinetics

356 Industrially, methanol is synthesized from syngas following the three main equilibrium reactions as  
 357 expressed by equations 3-5 over an industrial Cu/ZnO/Al<sub>2</sub>O<sub>3</sub> catalyst. However, it has been recently  
 358 agreed and demonstrated that methanol can also be produced from a feed with pure CO<sub>2</sub>/H<sub>2</sub> i.e., via equation  
 359 3 only even though the actual reaction mechanism and carbon source for methanol remains an active subject  
 360 of debate.<sup>10-13</sup>



364 Following Le'Chaterliers principle, higher methanol yields are favoured at lower temperatures and higher  
 365 pressures. However, for the reason of enhancing kinetics, temperatures in the range of temperature 200–  
 366 300 °C are used as well as high pressure ranges of 50-100 bar over the commercial Cu/ZnO/Al<sub>2</sub>O<sub>3</sub> catalyst.  
 367 The reverse water gas shift reaction (equation 4) is the only endothermic reaction in the three main reactions  
 368 and therefore gets promoted as temperature increases. This reaction increases the amount of water generated  
 369 in the case when pure CO<sub>2</sub>/H<sub>2</sub> is the main feed. This lowers the selectivity to methanol and the catalyst  
 370 activity. As a result, significant research efforts are devoted to the CO<sub>2</sub> hydrogenation to methanol process,  
 371 mostly to improve the catalyst conversion and selectivity.<sup>14-15</sup> However, the commercial Cu/ZnO/Al<sub>2</sub>O<sub>3</sub>-  
 372 based catalyst is likely to remain the best possible for some time due to its ability to achieve highest yield,  
 373 its low costs, and high stability.<sup>16</sup> Ruland et al. established, through dynamic experimental conditions  
 374 relevant to power-to-methanol (PtMeOH), that the industrial Cu/ZnO/Al<sub>2</sub>O<sub>3</sub> is highly stable for conditions  
 375 of chemical energy storage with hydrogen produced from fluctuating renewable energy sources, indicating  
 376 its relevance for application in PtMeOH.<sup>16</sup> Besides the challenges of optimizing the catalyst beyond what  
 377 the commercially available catalyst can achieve to promote CO<sub>2</sub>/H<sub>2</sub> to methanol, this reaction is attractive  
 378 from an environmental perspective in that a significant quantity of CO<sub>2</sub> can be recycled, and in addition it  
 379 is less exothermic, thus rendering ease of heat management in the reactor, and fewer by-products formation.  
 380 For these reasons and following the most recent kinetic analysis such as in the work of Nestler et al,  
 381 Slotboom et al., and de Oliveira Campos et al., who deduced that the role of CO hydrogenation to methanol  
 382 is negligible at high CO<sub>2</sub>/CO feed ratio, in this work and only reactions 3 and 4 are considered in the  
 383 modelling of the methanol synthesis.<sup>67-69</sup>

384 The kinetic model used in this study was presented in the work of Van-Dal & Bouallou.<sup>64</sup> which originated  
 385 initially from the model of Bussche and Froment.<sup>63, 65</sup> The model assumes methanol production from CO<sub>2</sub>  
 386 hydrogenation (i.e., equation 2) in the presence of RWGS as a competing reaction (equation 4) and absence





387 of diffusional limitations. Thus, the effectiveness factor equals 1. The kinetic model is based on Langmuir  
388 Hinshelwood Hougen-Watson (LHHW) kinetic model formulation and is expressed by equations 6 and 7.

$$389 \quad r_{CH_3OH} = \frac{k_1 P_{CO_2} P_{H_2} - k_6 P_{H_2O} P_{CH_3OH} P_{H_2}^{-2}}{\left(1 + k_2 P_{H_2O} P_{H_2}^{-1} + k_3 P_{H_2}^{0.5} + k_4 P_{H_2O}\right)^3} \left[ \frac{kmol}{kg_{cat}s} \right] \quad (6)$$

$$390 \quad r_{RWGS} = \frac{k_5 P_{CO_2} - k_7 P_{H_2O} P_{CO} P_{H_2}^{-1}}{1 + k_2 P_{H_2O} P_{H_2}^{-1} + k_3 P_{H_2}^{0.5} + k_4 P_{H_2O}} \left[ \frac{kmol}{kg_{cat}s} \right] \quad (7)$$

391 Where  $k_i$  were calculated for implementation in ASPEN PLUS V11® using the equation 8 and these are  
392 tabulated in Table 4 below.

$$393 \quad \ln k_i = A_i + \frac{B_i}{T} \quad (8)$$

394 Table 5 presents the main parameters of the distillation column which was modelled as RadFrac in ASPEN  
395 PLUS V11®.

396 All flowsheets used the same conditions, except only the distillation (DC) in flowsheet 2 in which the  
397 boilup ratio was set to 0.9 (lower) to ensure the methanol purity remains above 99wt%. NRTL-RK was  
398 selected as a property method to model the distillation column and its feed (with pressure  $\leq 1.1$  bar).

399

400 Table 4: Kinetic parameters rearranged for implementation in ASPEN PLUS V11® as a LHHW  
401 model.<sup>54,57</sup>

Kinetic parameters	Ai	Bi
$k_1$	-29.87	4811.2
$k_2$	8.147	0
$k_3$	-6.452	2068.4
$k_4$	-34.95	14928.9
$k_5$	4.804	-11797.5
$k_6$	17.55	-2249.8
$k_7$	0.1310	-7023.5

402

403 Table 5: Main parameters of the distillation column used for final separation of methanol.

Parameter	Value	Unit/basis
Column	RadFrac	-
Number of trays	30	-
Condenser type	Partial-Vapor-Liquid	-
Reflux ratio	1.5-1.62	mole
Boilup ratio	0.9- 1.5	mole
Feeding temperature	80	°C
Operating pressure	1.1	bar

404

405 Validation of the kinetic model is presented in the supplementary material section A2. The typical catalyst  
406 pellets of 6mm×4mm was packed in the catalyst bed and Ergun equation was used for pressure drop  
407 calculation through the catalyst bed. Following process engineering principles, the reactors were sized at



408 constant total reactor(s) volume. A hold-up time of 5 minutes was used in sizing the separators, and the  
409 compressor curves were used to model the compressors. Valves were modelled taking into consideration  
410 the typical efficiency relations and pressure drops. Thus, in modelling the different systems, the following  
411 summary of assumptions were made:

- 412 • An adiabatic fixed-bed tubular reactor has been used to convert CO<sub>2</sub> and H<sub>2</sub> into methanol. The  
413 overall CO<sub>2</sub>, H<sub>2</sub>O or H<sub>2</sub> feed is kept constant as in Table 1.
- 414 • The kinetics model and its parameters are kept constant. Where there are multiple reactors, the total  
415 reactor volume of all the reactors combined is kept constant similar to base case flowsheet 1 with  
416 one reactor as shown in the Supplementary Material section A3, Figure S3 and Section A5, Table  
417 S10. This keeps constant the total amount of catalyst used in all flowsheets, which is paramount  
418 for cost effective comparison.
- 419 • The reactor feed temperature is selected in the optimal temperature range (210<T<sub>in</sub><240) to  
420 optimise the temperature profile and conversion in the reactor.<sup>62</sup> Refer to the section A4  
421 (sensitivity-based optimisation) of the Supplementary Material.
- 422 • The by-products are negligible, and thus the produced materials in the reactor are methanol, CO,  
423 and water.
- 424 • Solar PV is used as a source of electricity. In the process, the water is used for cooling.
- 425 • Catalyst deactivation is negligible.
- 426 • The temperature of any flow or equipment is not considered lower than 20 °C, so that there is no  
427 need for a refrigerant cycle.
- 428 • The operating conditions have been selected with respect to the limitations of the industrial  
429 equipment and considering the outcomes of the design sensitivity analysis in section A4 of the  
430 supplementary material.
- 431 • In the hydrogen stream entering the process, 1.2 mol percent of water are considered.

### 432 2.2.2 System Configurations

433 It is important to highlight all flowsheet comprises a recycle loop, and the SOEC flowsheet was fixed for  
434 better comparison. Flowsheet 1 to 6B are shown in the supplementary material section A3 along with their  
435 brief description. To be concise, in this section, only the finally selected flowsheet 7, 7B and flowsheet 8  
436 are shown as these will be discussed in more details in the subsequent sections. Table 6 gives the description  
437 of the different flowsheets. The selection follows from the comparison with flowsheet 1 to 6B as described  
438 in the results section 3. Flowsheet 7 illustrated in Figure 3 includes two reactors connected in parallel  
439 followed by intermediate separation of methanol and series connection with the third reactor and thereafter,  
440 recovery of methanol from the recycle using two separators and a further separation of residual gases at



441 low pressure before the distillation column from which the final methanol product flows. Flowsheet 7B  
442 illustrated in Figure 4 has almost similar components as flowsheet 7 but the difference is that all reactors  
443 are connected in series. Flowsheet 8 illustrated in Figure 5 has three reactors connected in series, but the  
444 flowsheet is simplified series connection version of flowsheet 7B.

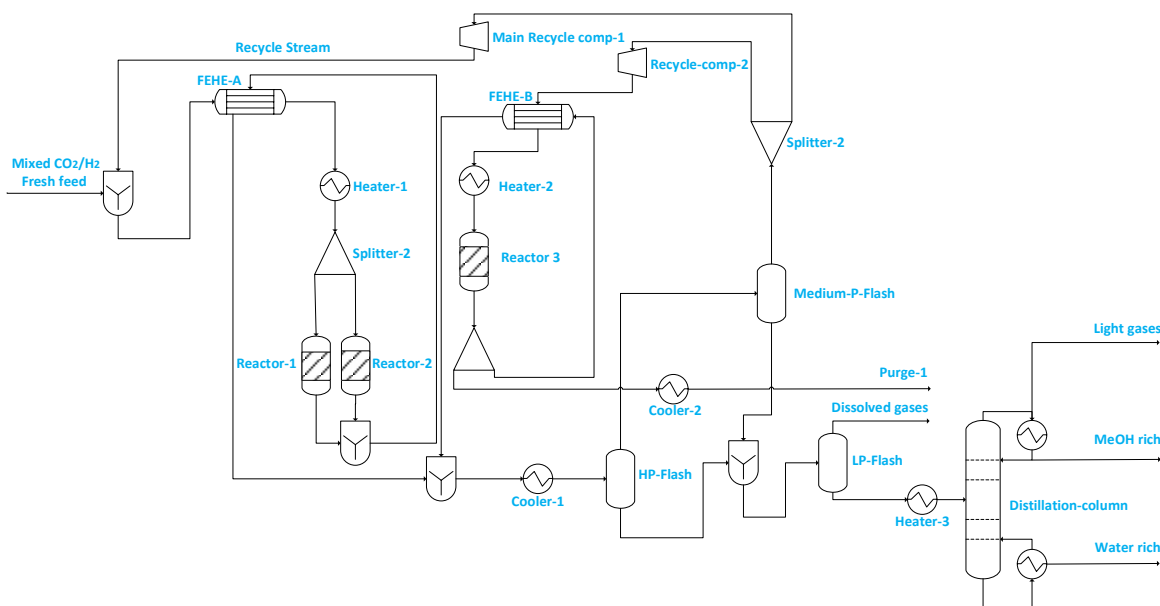
445 Table 6: Description of different flowsheets, their advantages, and limitations.

Process configuration	Description	Advantages	Limitations
Flowsheet 1	This is the base configuration with a single stage adiabatic reactor.	<ul style="list-style-type: none"> <li>• Simple configuration.</li> <li>• Less equipment and thus capital investment.</li> <li>• Simple start-up process.</li> </ul>	<ul style="list-style-type: none"> <li>• Large recycle stream is required for this process.</li> <li>• Low single pass conversion.</li> <li>• More valuable hydrogen purged.</li> </ul>
Flowsheet 2	Single stage reactor, with stripper column mounted before the reactor to enhance condensation and separation of methanol from CO <sub>2</sub> and remove water from the wet hydrogen feed.	<ul style="list-style-type: none"> <li>• Help to prevent catalyst deactivation from wet hydrogen.</li> <li>• Enhances the separation of dissolved gases from the methanol/water mixture.</li> </ul>	<ul style="list-style-type: none"> <li>• Large recycle stream is required for this process.</li> <li>• Low single pass conversion.</li> <li>• More valuable hydrogen purged.</li> </ul>
Flowsheet 3	Comprises two adiabatic reactors in series and with intermediate cooling and separation of methanol and water at 45 bar and 35°C. The other feature of flowsheet 3 is the addition of compressor to the feed of the second reactor to raise the operating pressure of the second reactor to the same pressure as the first reactor in the scheme.	<ul style="list-style-type: none"> <li>• Optimises the pressure to the second reactor and the overall pressure profile to enhance methanol production on the second reactor.</li> <li>• Enhances the conversion of the unconverted gases from the first stage.</li> <li>• Reduces the recycle stream.</li> </ul>	<ul style="list-style-type: none"> <li>• Increase number of equipment means more capital investment.</li> <li>• Repeated heating and cooling.</li> </ul>
Flowsheet 4	It has two reactors in series but with a wash column which uses C <sub>3</sub> H <sub>8</sub> O <sub>3</sub> as a solvent mounted in the position after the reactor followed by separation and two distillation columns in which the first is used for solvent recovery while the second distillation column is used for methanol purification.	<ul style="list-style-type: none"> <li>• This design enhances the driving force of the reaction by eliminating as much as possible the water and methanol from the unconverted gases.</li> <li>• Enhances the conversion of the unconverted gases from the first stage.</li> <li>• Reduces the recycle and compression work.</li> </ul>	<ul style="list-style-type: none"> <li>• Increase number of equipment means more capital investment.</li> <li>• Increased pressure drop with more reactors, and slightly increased compression.</li> <li>• Complexity and additional solvent recovery requirements.</li> <li>• Repeated heating and cooling.</li> </ul>
Flowsheet 5	Closely resembles flowsheet 3 with two reactors in series but with a change in operation of the intermediate separator which is operated at pressure equal to the reactor pressure to avoid the compression of the feed to the second reactor which comprises unconverted gases and some fraction of methanol.	<ul style="list-style-type: none"> <li>• Reduces compression work and recycle.</li> <li>• Enhances the conversion of the unconverted gases from the first stage.</li> </ul>	<ul style="list-style-type: none"> <li>• Increase number of equipment means more capital investment.</li> <li>• Increased pressure drop with more reactors, and slightly increased compression.</li> </ul>
Flowsheet 6A	Has two reactors connected in parallel. It also has long recycle to both reactors and therefore a feed (comprising fresh feed and recycle) split at 50% to both reactors.	<ul style="list-style-type: none"> <li>• Increases the residence time in each reactor and thus aims at enhancing the conversion.</li> <li>• Reduces the number of intermediate separators.</li> <li>• Reduces repeated heating and cooling.</li> </ul>	<ul style="list-style-type: none"> <li>• High recycle flowrate.</li> <li>• High compression requirements.</li> </ul>
Flowsheet 6B	Has two reactors connected in parallel. It has a short recycle in which the fresh feed flow is split to 50% and the portion of the fresh feed to the second reactor in flowsheet 6B is mixed with all the recycle of unconverted gases whereas the portion to the first reactor is kept as fresh feed.	<ul style="list-style-type: none"> <li>• Increases the residence time in first reactor and thus aims at enhancing the conversion.</li> <li>• Reduces the number of intermediate separators.</li> </ul>	<ul style="list-style-type: none"> <li>• High recycle flowrate</li> <li>• Relatively poor overall conversion.</li> <li>• Removes the recycle as a lever for temperature control in the first reactor especially for part-load operation.</li> </ul>
Flowsheet 7	Includes two reactors connected in parallel followed by intermediate separation of methanol and series connection with the third reactor and thereafter, recovery of methanol from the recycle using two separators and a further separation of residual gases at low	<ul style="list-style-type: none"> <li>• Increased reactants conversion and flexible loading/operation.</li> <li>• Reduced compression requirements, and hence potentially improved energy efficiency.</li> </ul>	<ul style="list-style-type: none"> <li>• Increase number of equipment means more capital investment.</li> <li>• Increased pressure drop with more reactors, and slightly increased compression requirement.</li> </ul>



Process configuration	Description	Advantages	Limitations
Flowsheet 7B	pressure before the distillation column from which the final methanol product flows. Has almost similar components as flowsheet 7 but the difference is that all reactors are connected in series. The feed to the third reactor is taken from the overall recycle stream and compressed further to boost the pressure.	<ul style="list-style-type: none"> <li>Reduced purge stream and hence CO<sub>2</sub> emissions.</li> <li>Increased reactants conversion.</li> <li>Reduced compression requirements, and hence potentially improved energy efficiency.</li> <li>Reduced purge stream and hence CO<sub>2</sub> emissions.</li> </ul>	<ul style="list-style-type: none"> <li>Complex start-up and shutdown with repeated heating and cooling.</li> <li>Increase number of equipment means more capital investment.</li> <li>Increased pressure drop with more reactors, and slightly increased compression requirement.</li> <li>Complex start-up and shutdown with repeated heating and cooling.</li> </ul>
Flowsheet 8	Has three reactors connected in series, but the flowsheet is a simplified series connection version of flowsheet 7B. This configuration has no booster compressor for the feed to all downstream reactors except the main recycle compressor feed.	<ul style="list-style-type: none"> <li>Increased reactants conversion.</li> <li>Reduced compression requirements, and hence potentially improved energy efficiency.</li> <li>Reduced purge stream and hence CO<sub>2</sub> emissions.</li> </ul>	<ul style="list-style-type: none"> <li>Increase number of equipment means more capital investment.</li> <li>Increased pressure drop with more reactors, and slightly increased compression requirement.</li> <li>Complex start-up and shutdown with repeated heating and cooling.</li> </ul>
Co-electrolysis flowsheet	Has three reactors connected in series, similar to flowsheet 8. The main difference is the upstream steam-electrolysis step which is replaced to co-electrolysis and thus leading to fresh feed to the reactor with syngas instead and increased CO concentration.	<ul style="list-style-type: none"> <li>Existing catalyst optimised for the syngas feed.</li> <li>Co-electrolysis step enhances the energy efficiency of system.</li> <li>Enhanced conversion with the introduction of CO.</li> </ul>	<ul style="list-style-type: none"> <li>Would practically results in the more impurities and difficulties in downstream separation as the existing industrial syngas systems.</li> <li>Selectivity to methanol decreases with increase in CO/CO<sub>2</sub> ratio.</li> </ul>
e-RWGS flowsheet.	Has three reactors connected in series, similar to flowsheet 8. The main difference is the upstream steam electrolysis step which is coupled e-RWGS and thus leading to fresh feed to the reactor with syngas instead, and increased CO concentration.	<ul style="list-style-type: none"> <li>Enhanced conversion with introduction of CO.</li> <li>Existing catalyst optimised for the syngas feed.</li> <li>Higher CO/CO<sub>2</sub> ratio leads to higher methanol production.</li> </ul>	<ul style="list-style-type: none"> <li>Would practically results in the more impurities and difficulties in downstream separation as the existing industrial syngas systems.</li> <li>Selectivity to methanol decreases with increase in CO/CO<sub>2</sub> ratio.</li> <li>Required separation of water formed from e-RWGS reactor.</li> </ul>

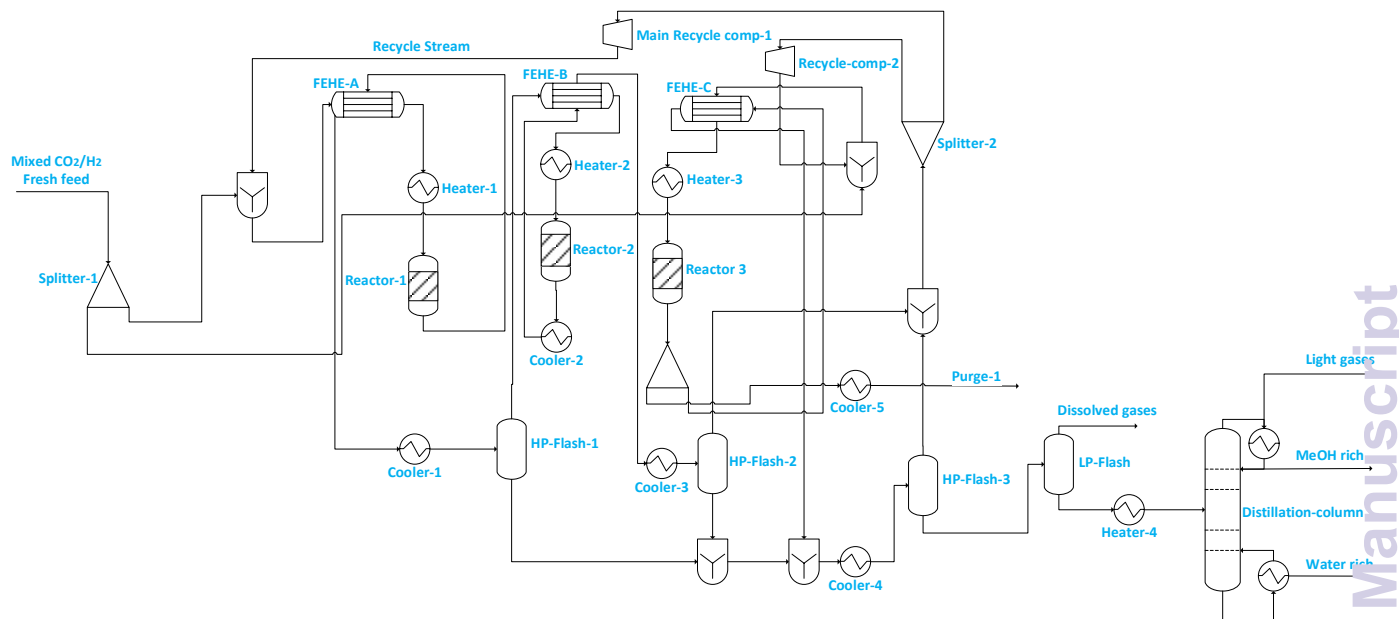
446



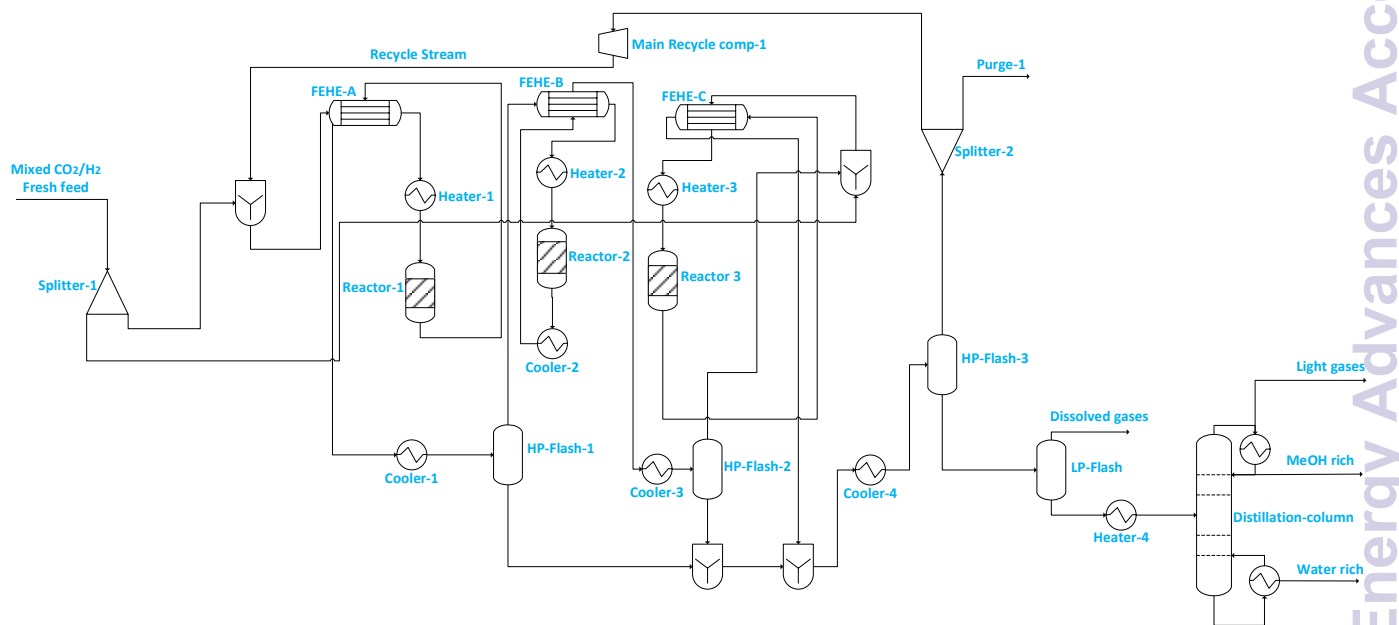
447

448 Figure 3: Illustration of Flowsheet 7. This flowsheet features parallel-series configuration of the three  
449 adiabatic reactors.





450  
451 Figure 4: Illustration of Flowsheet 7B. This flowsheet features three reactors in series with intermediate  
452 cooling. This features a different feed, product-purge arrangement to the third reactor (reactor 3).



453  
454 Figure 5: Illustration of Flowsheet 8. This flowsheet features three adiabatic reactors in series with  
455 intermediate cooling.

### 456 2.3 Dynamic reactors system modelling for flexibility analysis

457 Three of the most promising reactor configurations were selected and assessed in comparison for their  
458 flexibility analysis. The loads were varied from minimum to maximum (i.e., 40-102%) with consideration



459 of practicality in the design of the equipment such as pumps, compressors (e.g., to prevent surge and  
460 stonewall), etc. Dynamic modelling of the methanol synthesis section is conducted using the ASPEN  
461 DYNAMICS V11®. The initial state of the different reactor configurations were extracted from steady-  
462 state simulations conducted using Aspen Plus by means of pressure driven approach leading to a more  
463 realistic model comparable to real plants. The flowsheets after dynamic translations (with all critical control  
464 loops) are shown in the supplementary material, section A4.1. The dynamics of the process are highly  
465 dependent on the reaction kinetics and modelling approaches.<sup>34</sup> For the dynamic simulation, the distillation  
466 section is excluded following the findings from Cui et al. that distillation dynamics, which affects the  
467 product quality, is easy to manage under variable loads.<sup>66</sup> For the methanol synthesis, the feed H<sub>2</sub> and CO<sub>2</sub>  
468 were mixed at stoichiometric ratio of H<sub>2</sub>/CO<sub>2</sub> = 3, before being mixed further with the recycle stream.

469 Signal generators were used during the dynamic modelling, to alter the rates of flow change (i.e., load  
470 change) for the feed gases. Moreover, tuned proportional–integral (PI) controllers were used for dynamic  
471 operation. The proportional and integral gains were tuned based on the Ziegler-Nichols and Tyreus-Luyben  
472 tuning rules by using the automatic controller tuning in ASPEN DYNAMICS V11®. Details of the tuned  
473 controllers are shown in the supplementary material. The systems are evaluated considering the KPIs such  
474 as energy efficiency, flowrate of the feed streams (i.e., load change), reactor conversion, heat duties and  
475 power of the compressors. The hydrogen produced from the renewable electricity and methanol represents  
476 the major power input and output, respectively.

#### 477 **2.4 Technical performance indicators**

478 The mass and energy balance of the process configurations were calculated. The selected indicators to  
479 evaluate the studied processes including the overall CO<sub>2</sub> conversion, energy efficiency, production rate, and  
480 load change are used as criteria for comparisons. The energy efficiency expressions of the SOEC system,  
481 and the overall system defined below, follows from the work of Lonis et al. and Cui et al.<sup>59–60, 66</sup> For the  
482 SOEC unit operating to produce hydrogen or syngas as the key product, equation 9 describe the expression  
483 for the efficiency the water electrolysis section.

$$484 \quad \% \eta_{SOEC, product} = \frac{\dot{m}_{product} \times LHV_{product}}{P_{SOEC} + P_{BOP,SOEC}} \quad (9)$$

485 Where  $\dot{m}_{product}$  refers to the mass flowrate of hydrogen or syngas (for co-electrolysis),  $LHV_{product}$  refers to  
486 the lower heating value of hydrogen or syngas,  $P_{SOEC}$  refers to the electric power of the SOEC while  
487  $P_{BOP,SOEC}$  is the power of the SOEC auxiliaries. Single pass conversion of carbon is expressed by equation  
488 10. The CO is considered in the calculation of single pass conversion since the feed to the reactor contains  
489 CO introduced by recycle although the overall system boundary feed to the process doesn't contain CO but





only CO<sub>2</sub> and H<sub>2</sub>O. The efficiency of the integrated SOEC and the methanol synthesis i.e., the PtMeOH efficiency can be described using equation 11.

$$\% \eta_{C, conversion} = \frac{(CO_{2, in} + CO_{in}) - (CO_{2, out} + CO_{out})}{(CO_{2, in} + CO_{in})} \quad (10)$$

$$\% \eta_{PtMeOH} = \frac{\dot{m}_{MeOH} \times LHV_{MeOH}}{P_{SOEC} + P_{BOP, SOEC} + E_{MSS} + P_{BOP, MSS}} \quad (11)$$

Where  $E_{MSS}$  refers to the heat energy requirements in the methanol synthesis unit (MSS) i.e., for preheating the feed to the reactor and distillation column, and for reboiler in the distillation. The  $\dot{m}_{MeOH}$  (kg/h) is the mass flow rate of the streams,  $LHV$  is the lower heating value for the gases, and  $P$  represents the heat duty of the heat exchangers or the power inputs for the recycle compressor and pumps. Furthermore, heat integration is also considered for all the most promising flowsheets and thus the composite curves and exchanger designs are investigated. Heat integration eliminates/reduces external heat requirements in the methanol synthesis and distillation section (i.e., yield to  $E_{MSS} \approx 0$ ). A brief analysis of the impact of heat integration on the three selected flowsheets (flowsheet 7, 7B and 8) is presented in section A4.3 of the Supplementary material.

### 3. RESULTS AND DISCUSSION

#### 3.1 Electrolyser performance: steam vs co-electrolysis

Table 7 summarises the energy balance pertaining the heating and cooling within the SOEC system. High temperature SOEC) has an advantage in terms of having higher energy efficiency. This is because this technology utilises both heat and electricity. In general, the higher the temperature the lower the electricity demand. On the other hand, increasing the temperature reduces the overvoltage losses i.e., the ohmic losses. Therefore, the SOEC exhausts (anode and cathode) are used to preheat and superheat the feed streams containing recirculated oxygen sweep gas and demineralized water.

Table 7: Energy balance in the SOEC section under steam electrolysis.

Heating process	Heat (kW)	T <sub>in</sub> (°C)	T <sub>out</sub> (°C)	Cooling process	Heat (kW)	T <sub>in</sub> (°C)	T <sub>out</sub> (°C)
Sweep air PH by heat recovery (FEHE6)	116	248	650	Anode exhaust 1st cooling (FEHE6)	-113	850	831
Sweep air SH by external source (Heater3)	61	650	850	Anode exhaust 2 <sup>nd</sup> cooling (FEHE4)	-1273	831	619
Water PH and VAP external heat (Heater1)	21602	28	180	Anode exhaust 3 <sup>rd</sup> cooling (FEHE2)	-137	619	595
Water SH by heat recovery (FEHE1)	2422	180	332	Anode exhaust 4 <sup>th</sup> cooling (ANOD-COOL)	-2587	595	130
Water SH by heat recovery (FEHE2)	137	332	340	Cathode exhaust 1 <sup>st</sup> cooling (FEHE5)	2110	850	707
Water SH by heat recovery (FEHE3)	2755	340	505	Cathode exhaust 2 <sup>nd</sup> cooling (FEHE3)	-2755	707	515
Steam SH by heat recovery (FEHE4)	1273	505	579	Cathode exhaust 3 <sup>rd</sup> cooling (FEHE1)	-2422	515	342
Water SH by heat recovery (FEHE5)	2111	579	697	Cathode exhaust 1 <sup>st</sup> cooling (CAT-COOL)	-9023	342	35
Steam SH by external heat (Heater 2)	2835	714	850				

SH=super heat, VAP=vaporisation, PH=preheating



513 Additional external heat source is still required to preheat and vaporise demineralized water, and further  
 514 raise the temperature of the demineralized steam and sweep gas to the SOEC operating temperature (850  
 515 °C). Table 8 summarises the performance of the steam and co-electrolyser considering the power  
 516 consumption and energy efficiency. The steam electrolysis-based SOEC required to produce about 1213  
 517 kmol/h of hydrogen under the operating conditions stipulated in Table 2, a corresponding electrical power  
 518 of approximately 109 MW is required. Since the electrolyser is operated at thermoneutral voltage, the  
 519 efficiency is high due to negligible overpotential losses compared to endothermic operation.<sup>55</sup> The steam-  
 520 based SOEC system efficiency value of  $\eta_{\text{soec,system}} = 74.5\% - 78.2\%$  obtained in this work is comparable to  
 521 values that have been reported in literature for the SOEC efficiency values<sup>52-53, 55-56</sup> at thermoneutral voltage  
 522 such as the value ( $\eta_{\text{soec,system}} = 83\%$ ) which was presented in the work of Lonis et al. who used the definition  
 523 of energy efficiency similar to equation 9 above, even though the model for SOEC was fairly simplified in  
 524 this work.<sup>60</sup> The slight under-estimation of efficiency in this work is perhaps due to the differences in model  
 525 formulation. However, the results are very comparable to what literature reports for SOEC energy  
 526 efficiency at thermoneutral voltage<sup>52-53, 55-56</sup> and thus giving confidence about the relevance of model  
 527 formulation assumptions in this work. On the other hand, the co-electrolysis based SOEC efficiency  
 528 considering the BOP energy consumption was found to be around  $\eta_{\text{soec,system}} = 76 - 79\%$  and comparable to  
 529 literature.<sup>32, 55</sup> The power consumption in co-electrolysis mode is however higher than that in the steam  
 530 based SOEC mode and this trend is similar to that found by Patcharavorachot et al.<sup>50</sup> This is because in co-  
 531 electrolysis mode, both H<sub>2</sub>O and CO<sub>2</sub> conversion reactions consume electrical power.<sup>50</sup>

532 Table 8: Performance of the electrolyser system for steam electrolysis and co-electrolysis

Parameter/index	Units	Steam-electrolysis	Co-electrolysis
		Value	Value
LHV (H <sub>2</sub> or CO+H <sub>2</sub> )	MJ/kg	120	25
P <sub>soec</sub>	MW	84	107
P <sub>soec,BOP</sub>	MW	25	27
$\eta_{\text{soec,system}}$	%	74.5	76.2
$\eta_{\text{soec,system,R}}$	%	78.2	79.2

533  
 534 However, for the co-electrolysis-based mode, a slightly higher (1.7% more than water-electrolysis mode)  
 535 overall SOEC system energy efficiency was obtained for the same ratio. This is mainly due to reduced feed  
 536 steam requirements in co-electrolysis mode, as part of the steam is produced from CO<sub>2</sub> to CO reaction (i.e.,  
 537 RWGS). It is also critical to highlight that the hot streams from the SOEC have been used only for the  
 538 heating of the cold streams in the SOEC section to avoid complications of the process and to better assess  
 539 the influence of the configured methanol synthesis section on the overall energy efficiency of the process.  
 540 This renders the two system thermally independent, which is advantageous when variable renewable



541 electricity is used in PtMeOH, provided this is achieved at minimal possible cost. This allows for some  
542 degree of flexible part-load operation for each section with reduced regulation or operation issues.

543 As also highlighted by Chen and Yang et al., integration of heat between two or more subsystems should  
544 be minimized unless otherwise necessary, and optimal integration (also reducing heat curtailments) within  
545 a subsystem should be maximised.<sup>31</sup> For the final heating of the steam via heater 3, an external source is  
546 required (e.g. electricity) in order to achieve the operating conditions of the SOEC. An alternative would  
547 be to operate the electrolyser above thermoneutral point and thus use the surplus heat from overpotentials,  
548 but this is not considered in this study as it adversely promotes cell degradation. External electrical heat  
549 requirements for the SOEC section ( $\approx 24\%$  of the total electrolysis power) is needed to generate superheated  
550 steam and heat the sweep gas to the SOEC temperature. The sweep gas must first be compressed and heated  
551 to the SOEC temperature.

### 552 **3.2 Methanol Production Rate, Energy Efficiency, Overall and Single-pass CO<sub>2</sub> and H<sub>2</sub>** 553 **Conversion**

554 Comparison of the process flowsheet configurations based on methanol production rate, energy efficiency,  
555 carbon conversion and H<sub>2</sub> conversions are shown in Figure 6, Table 9 and 10. The overall CO<sub>2</sub> conversion  
556 is calculated considering a recycling system in all configurations. Comparison of the methanol production  
557 rate shows that three reactors, gives higher methanol production rate. The highest methanol production rate  
558 is found for flowsheet 7B which comprises of three reactors in series with intermediate cooling and  
559 separation. Comparison of the process flowsheets (see Figure 6) depicts that configuration expressed as  
560 flowsheet 5 has a slightly higher energy efficiency. Flowsheet 7B has a similar overall CO<sub>2</sub> and H<sub>2</sub>  
561 conversion and energy efficiency as flowsheet 7 and flowsheet 8. However, the flowsheet 7B differs slightly  
562 (about 1% less) in terms of the energy efficiency compared to flowsheet 5. Table 9 shows the single pass  
563 CO<sub>2</sub> conversion of each reactor per flowsheet configuration. Since the process configuration of flowsheet  
564 1 and 2 follows from the work of Van-Dal & Bouallou and Kiss et al. the single pass CO<sub>2</sub> conversion from  
565 this work are comparable to those of Van-Dal & Bouallou and Kiss et al. for flowsheet 1 and 2,  
566 respectively.<sup>54,58, 63</sup> The reason the flowsheets 1 and 2 were re-modelled in this work was to ensure fair  
567 comparison using similar scale and process conditions since the original work of Van-Dal and Bouallou  
568 and Kiss et al. used distinct conditions and/or target production capacities and kinetics.<sup>61, 64, 70</sup> Even if the  
569 capacities were to be similar, different operating conditions will yield different performance. Single pass  
570 conversion in series reactors with intermediate cooling shows an increasing trend as reactor stages increase.  
571 This is so as the removal of water and methanol via intermediate cooling and separation increases the  
572 driving force of the CO<sub>2</sub> conversion reaction and thus enhances CO<sub>2</sub> conversion. Although flowsheet 2 can  
573 produce a high methanol comparable to flowsheet 7, 7B and 8, it has a slightly lower energy efficiency.



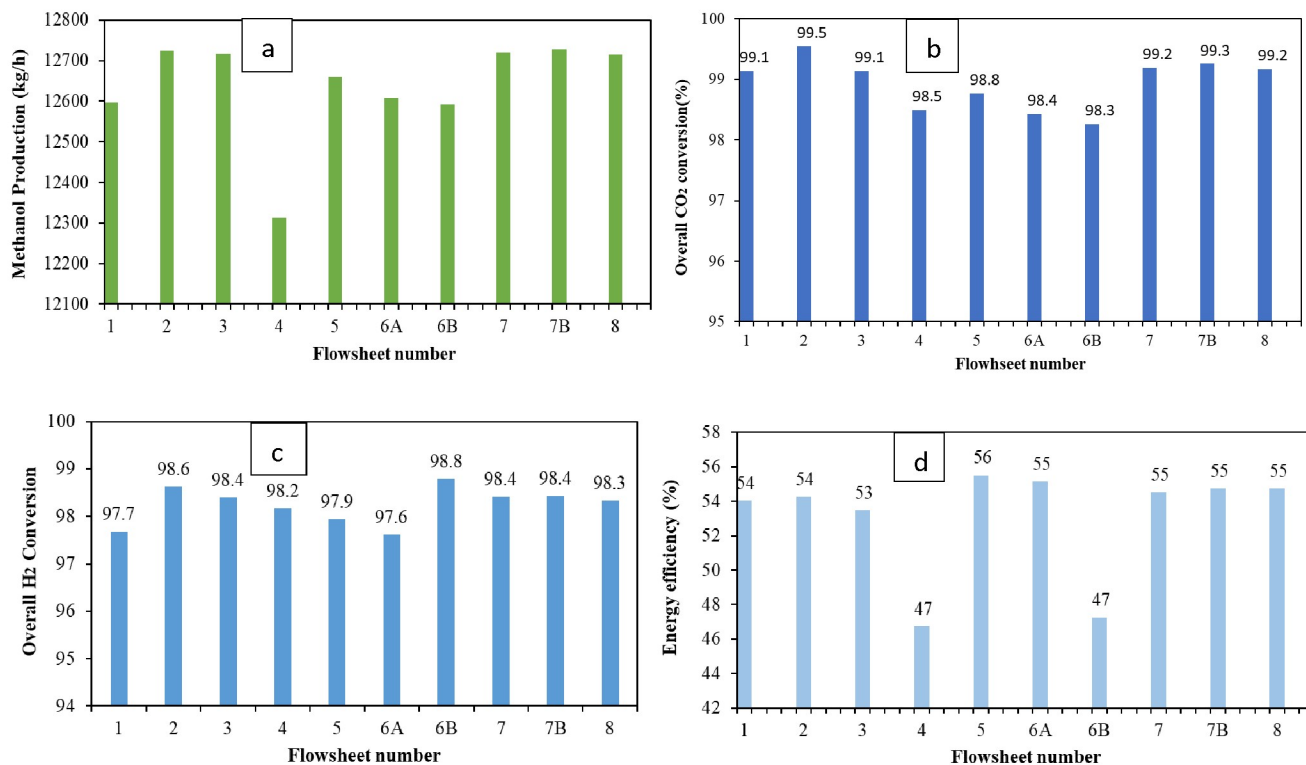


Figure 6: Performance of the different flowsheet considered in this paper: (a) methanol production. (b) overall CO<sub>2</sub> conversion. (c) Overall H<sub>2</sub> conversion. (d) Overall energy efficiency of the process.

Table 9: Single pass carbon conversions of each reactor in the evaluated process configurations.

Reactor (R)	Flowsheet number									
	1	2	3	4	5	6A	6B	7	7B	8
	% CO <sub>2</sub> Conversion in each reactor in the flowsheet									
R1	39.1	17.8	39.7	39.0	40.4	42.0	47.4	51.5	32.8	30.3
R2	-	-	53.6	53.9	55.8	42.0	10.1	51.5	42.8	40.3
R3	-	-	-	-	-	-	-	34.5	50.2	46.6

Table 10: Single pass H<sub>2</sub> conversions of each reactor in the evaluated process configurations.

Reactor (R)	H <sub>2</sub> % conversion per flowsheet number per reactor									
	1	2	3	4	5	6A	6B	7	7B	8
R1	9.3	18.6	8.6	9.2	9.2	9.2	8.1	7.0	11.1	11.2
R2	-	-	6.7	7.0	6.5	9.2	4.3	7.0	9.6	10.0
R3	-	-	-	-	-	-	-	10.2	7.6	7.5



575 Despite effort to recover as much methanol in flowsheet 4 with additional separation via solvent wash  
 576 column, the overall methanol production and energy efficiency is not improved for this process. This is  
 577 because thermodynamically limits on recoverable methanol in a given stream. This process may also  
 578 introduce losses of valuable reactants that may otherwise be recycled and reconverted. For parallel reactors  
 579 having a short recycle stream, similar to configuration in Flowsheet 6B, slightly decreases the overall  
 580 methanol production rate and CO<sub>2</sub> conversion. The short recycle also results in large recycle stream and  
 581 hence increased recycle compressor duty. This decreases the energy efficiency and hence flowsheet 6B has  
 582 low energy efficiency as indicated in Figure 6d. When these parallel reactors are designed with a long  
 583 recycle (flowsheet 6A) and equally divided feed each reactor has a single pass conversion slightly higher  
 584 than flowsheet 1 & flowsheet 2 which is expected because a smaller mole flowrate of the reactants is fed  
 585 for comparable catalyst mass inside these reactors, thus resulting into higher residence time and hence  
 586 increased carbon conversion.

587 Table 11: Comparison of the energy efficiency obtained from this study and those found in literature.

Reference	Energy efficiency (%) w/o heat integration
Hank et al. <sup>12</sup>	40.2-44.1
Rivera Tinoco et al. <sup>14</sup>	54.8
Szima & Cormos <sup>71</sup>	53.93
Bos et al. <sup>15</sup>	50
Parigi et al. <sup>72</sup>	58.8
This study	Flowsheet 5: 56 Flowsheet 7: 55 Flowsheet 7B: 55 Flowsheet 8: 55

588  
 589 The trend of conversion with changes in flowrate is also observable when reactors are staged in series with  
 590 intermediate cooling. The rapid increase in the conversion of R3 corresponding to Flowsheet 7B is a result  
 591 of significant reduction in its feed flow-rate since the series staging of the reactors converts more of the  
 592 reactants (overall, each reactor in the earlier stages receive higher flows) and the subsequent intermediate  
 593 segregation of methanol and water which increase the driving force on reactor R3. In addition, the analysed  
 594 process conversion is higher due to absence of impurities in the feed. The results are comparable to the  
 595 findings of Basonde & Urakawa, who experimentally demonstrated the similar single pass CO<sub>2</sub> conversion  
 596 using 10:1 H<sub>2</sub>/CO<sub>2</sub> feed.<sup>73</sup> The performance that would be achieved with 3.333 times more hydrogen  
 597 (expensive to make from electrolysis) than the stoichiometric ratio in the feed is the same as having the  
 598 configurations as discussed with the H<sub>2</sub>/CO<sub>2</sub> of 3:1 in the overall feed. Thus, the reactor configuration  
 599 strongly influences the conversion of CO<sub>2</sub> to methanol.

600 Hydrogen storage is another key goal of the PtMeOH process. In this regard, the storage of hydrogen is  
 601 assessed in terms of the amount of hydrogen that is converted to methanol in the process. Viewed from the



602 overall process-based hydrogen conversion as depicted in Figure 6, methanol production using flowsheet  
603 6B with short recycle had a higher overall H<sub>2</sub> conversion. This is achieved without application of hydrogen  
604 gas recovery, e.g. membranes, which are often applied industrially to increase the overall conversion of  
605 hydrogen. The use of membrane was not considered in this paper due to its potential to increase the methanol  
606 production cost. Table 10 shows the single pass conversion of hydrogen to methanol. The single pass  
607 conversions of hydrogen are lower than the CO<sub>2</sub> single pass conversions since hydrogen is always in excess  
608 in the feed of the reactor due to a significant amount of it in the recycle.

609 Figure 6 also plots the energy efficiency of the flowsheets. The trend without heat integration shows that  
610 flowsheet 5 has the highest energy efficiency followed by flowsheet 7, 7B and 8. However the production  
611 rate of flowsheet 5 is slightly lower than those of flowsheet 7, 7B and 8. This is because flowsheet 7, 7B  
612 and 8 have the additional reactor which converts more materials and thus have a slightly higher production  
613 rate. This shows a trade-off between the energy efficiency and the production rate. As the production rate  
614 increases energy efficiency decreases slightly. For flowsheet 5, the intermediate flash drums for separation  
615 of methanol and water from unconverted gases are operated at high pressures. This in effect reduces the  
616 energy requirements and size of the compressors to the second reactor and recycle. This depicts a trade-off  
617 between compression cost and flash drum pressure as observed by Luyben et al.<sup>9</sup> This implies that caution  
618 must be taken to avoid increasing pressure excessively in a way that the contents of unconverted gases and  
619 inert in the liquid stream sent to the distillation column increases (thus reducing the quality of the product)  
620 or significantly reducing the pressure and thus increasing the compression requirements of the recycle  
621 compressor. The flowsheet 7, 7B and 8 have the same energy efficiency (see Table 11). Thus, this indicates  
622 a trade-off, between production rate and energy requirements which has been articulated by several other  
623 authors.<sup>22, 56</sup> However, looking at the temperature profile at the exit of the reactor in flowsheet 7, 7B, 8  
624 opportunities for heat integration exist and could improve the energy efficiency of the process. Mechanical  
625 work and process heating (excluding the integrated heating) in this work are powered by electricity only.  
626 Energy efficiencies are still low, and this indicates the need to perform heat integration analysis and heat  
627 exchanger network design which is summarily performed and discussed in section A4.3 of the  
628 supplementary material. Before performing heat integration, sensitivity-based optimisation of the reactor  
629 section of the flowsheets is investigated for flowsheet 7, 7B and 8 to determine the optimal operating  
630 conditions associated. The results of the design sensitivity are shown in section A4.2 of the supplementary  
631 material. Sensitivity on critical parameters such as the recycle ratio, fresh feed partitioning, feed  
632 temperature reactor, separator pressure and temperature were performed. The findings show that fresh feed  
633 partitioning does not change the methanol production rate but can influence the control of the hot spot  
634 temperature and offer a degree of freedom under dynamic operation. From the heat integration, the series-  
635 series configuration showed low utility requirements upon optimisation of the heat exchanger network.





### 636 3.3 Assessment of flexibility of the methanol synthesis section

#### 637 3.3.1 Feed flowrate and product streams

638 Generally, reactor configurations influence the flexibility of the process.<sup>32</sup> In this section, both parallel-  
639 series and series-series based configuration are assessed. Both series- and parallel-series-based  
640 configurations with three reactors are modelled under dynamic conditions by changing the load (feed  
641 flowrate). Simultaneous modulation of the CO<sub>2</sub> and H<sub>2</sub> feed is performed to maintain the CO<sub>2</sub>:H<sub>2</sub> ratio of  
642 1:3 in the feed. In a cascade series-series reactor design (i.e., flowsheet 7B, 8 and syngas-based flowsheet),  
643 changes in the conversion and temperature in one stage influences the reaction rate of the next stage. The  
644 non-linear relationship of temperature and concentration may render some intermediate load points  
645 infeasible, even though the minimum and maximum may be feasible. However, this was found to not be  
646 the case for all the four designs considered in the present study. The minimum and maximum loads used in  
647 this study are  $\beta_{min} = 40\%$  and  $\beta_{max} = 105\%$  for flowsheet 7, 7B and 8. While the syngas-based  
648 flowsheets had the minimum allowable load-change of 45% of the nominal. Below these  $\beta_{min}$  values, the  
649 Aspen Dynamics integrator fails. The part-load refers to 50% of nominal load. In this study, a load ramp  
650 (R) of 60% load per hour and a total time on stream of 15 hours were considered. Figure 7 shows effect of  
651 load change from full-load to part-load on flowrates of the main feed and product streams. A linear decrease  
652 in the flowrate from full-load to part-load occurs during t=1–2.19 h and linear from full-load to part-load  
653 increase from t=5–9.51 h is depicted. This is desirable as it promises quick and good response to process  
654 variability under intermittent renewable energy. As expected, following the previous study on a single  
655 reactor by Cui et al. both the methanol production rate and the purge stream follows the same trend of the  
656 load change.<sup>66</sup>

657 All three configurations had the relatively comparable process flexibility; meaning they all  
658 achieved/tolerated minimum to full load operation without any violation of path constraints such as  
659 maximum allowable temperature in the reactors. However, it took 1.08, 1.16 and 1.19 h to reach the part-  
660 load steady state for flowsheets 7, 7B and 8, respectively. To reach the full load steady state from the part-  
661 load conditions, it took 1.51, 3.21 and 4.51 h for flowsheet 7, 7B and 8, respectively. Small undershoots  
662 and overshoots are observed on the purge stream for all flowsheet at minimum load. Although these  
663 flowsheets can handle the load change very well, parallel-series configuration (flowsheet 7) seems to be  
664 attractive with the ability to reach steady state faster. For all flowsheets, dual control (split range control)  
665 of the recycle split ratio (see flowsheets details on the supplementary material) was necessary to reach low  
666 load levels and hence dynamize the methanol synthesis section. In Figure 7B, there is an overshoot in the  
667 purge after part-load operation and it took longer than 24 hours for the purge in this flowsheet to stabilise  
668 to the initial steady state value. When comparing the CO<sub>2</sub> hydrogenation-based flowsheet to the syngas-



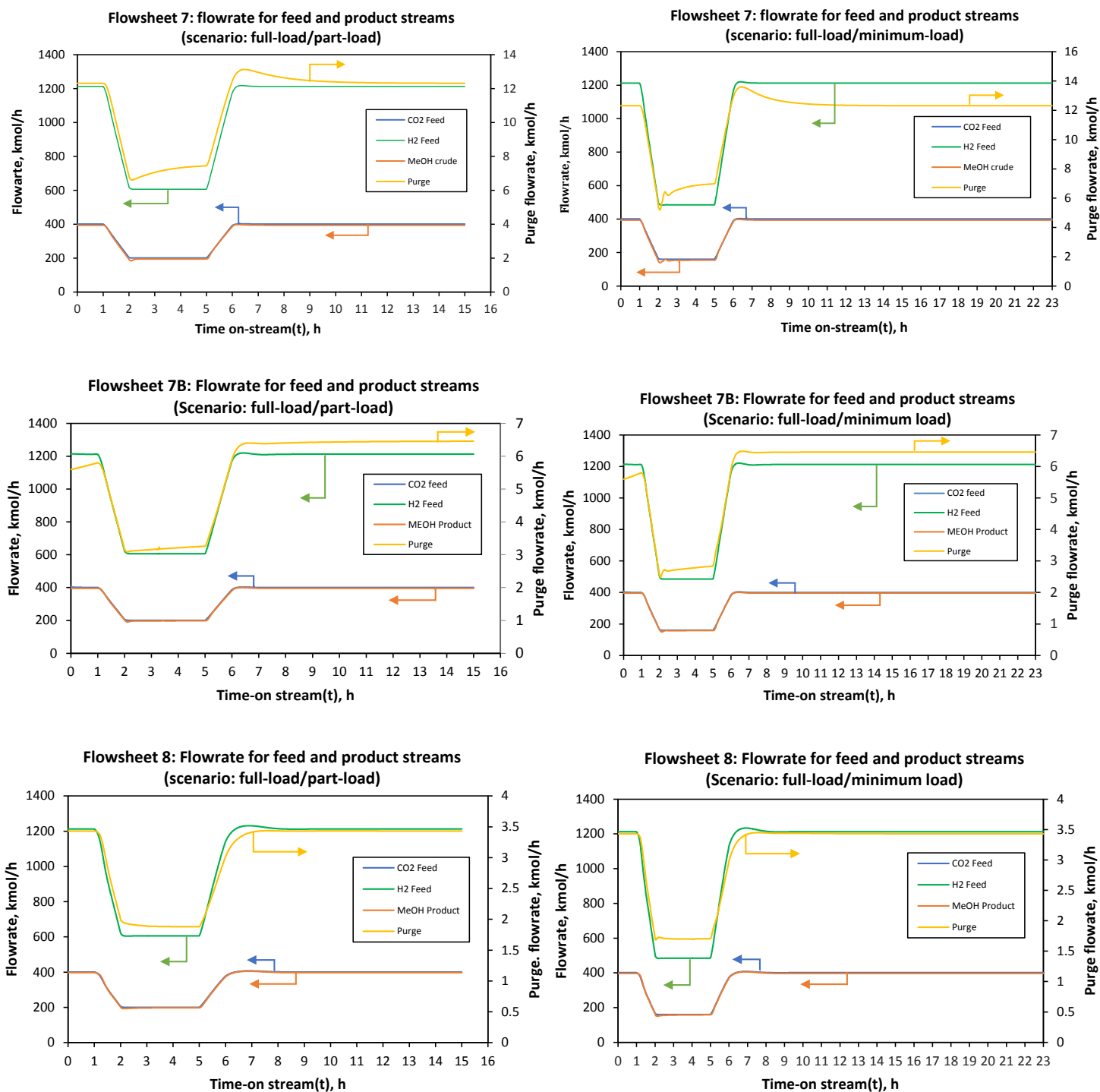


Figure 7: Shows the flowrate of the feed and the product streams when the load was changed from full-load (100%) to part-load (50%) and minimum load (40%). These results are for flowsheet 7, flowsheet 7B and flowsheet 8.

669

670 based flowsheets as depicted by Figure 8, the CO<sub>2</sub> hydrogenation had better load flexibility than the syngas-  
 671 based flowsheet, even though the architecture of syngas-based flowsheet is similar to series-series flowsheet  
 672 8. However, operation at loads higher than nominal is possible (up to 110% for syngas-based flowsheet).

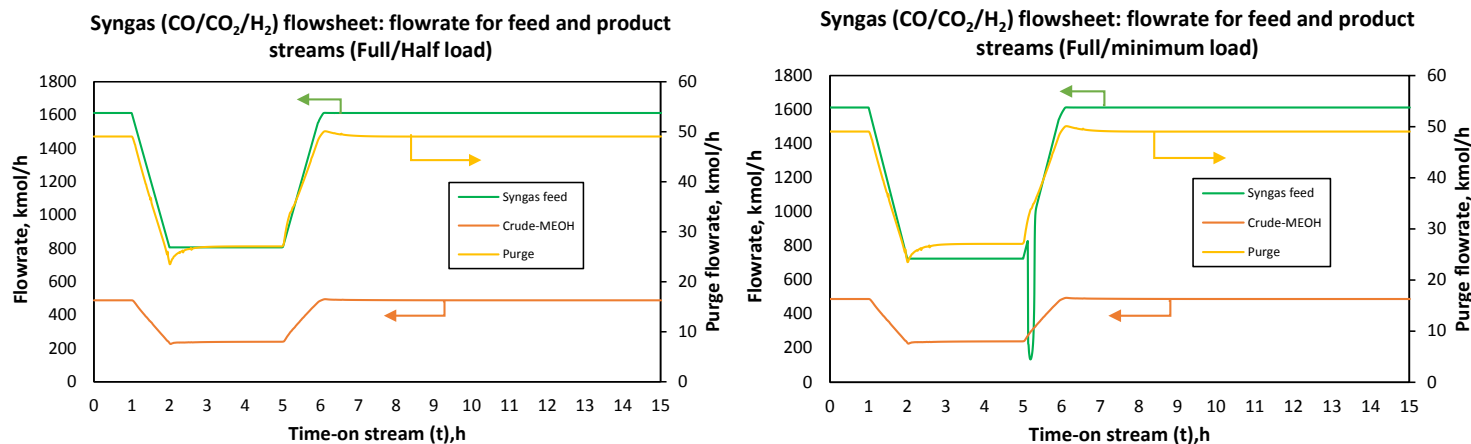


Figure 8: Shows the flowrate of the feed and the product streams when the load was changed from full-load (100%) to part-load (50%) and minimum load (45%) for co-electrolysis derived syngas to methanol.

673 Syngas-based flowsheet was also marred by the instabilities at minimum load, where undershoot were  
 674 observed on the purge and syngas-feed when the load was ramped from the full-load to part-load and  
 675 minimum loads to full-load. It also takes a while for the recycle splitter to maintain the split ratio and hence  
 676 the observed drops in the purge stream. Any flowrate within the defined load range can be reached  
 677 successfully, safely and without system shutdown when the control system is properly designed. The  
 678 change in the adiabatic reactors exit temperatures with the load change was almost negligible for the CO<sub>2</sub>  
 679 hydrogenation reaction. This is because as the feed flowrate is increased or decreased, the heat released is  
 680 distributed across the reactor at higher feed flow, and the reverse water-gas shift reaction which gets more  
 681 promoted at high residence time balances out the heat released at reduced flow. One would expect that with  
 682 more methanol production more heat will be released in the reactors, but this is mitigated by these factors.  
 683 In addition, the large recycle stream also causes the balancing effect providing the necessary temperature  
 684 control and distribution. However, the potential effects of inaccuracies of the steady state kinetic model  
 685 used to simulate the dynamic thermal profile must be investigated further. The current results shows that  
 686 the storage capacity between the methanol synthesis reactors and the upstream process (electrolysis and  
 687 CO<sub>2</sub> capture) can be reduced at-least to allow for operation in the defined load range (40-100%). Lower  
 688 part-load are expected to be problematic more especially for the syngas-based process since the increase in  
 689 residence time results into higher heat evolution inside the reactors creating possibility of hot-spot  
 690 formation. However, the final decision on the design of the feed storage capacity(s) on the upstream of the  
 691 first stage reactor will be detected by the economic feasibility of each point. The economics under dynamic  
 692 conditions are not considered in this study. Regardless, it is clear from the analysis in this study that  
 693 methanol synthesis via adiabatic reactors can operate over an extended load range comparable with  
 694 adiabatic reactors for methanation reaction.<sup>32</sup>



695 **3.3.2 Composition of the feed**

696 The composition of the feed of the reactor varies with load change as depicted in Figure 9. For the parallel  
697 –series and series-series configuration, the CO<sub>2</sub>, methanol, H<sub>2</sub>O and CO molar content in the feed of all the  
698 three reactors decreases with decrease in load; interestingly following the same trend as the load change.

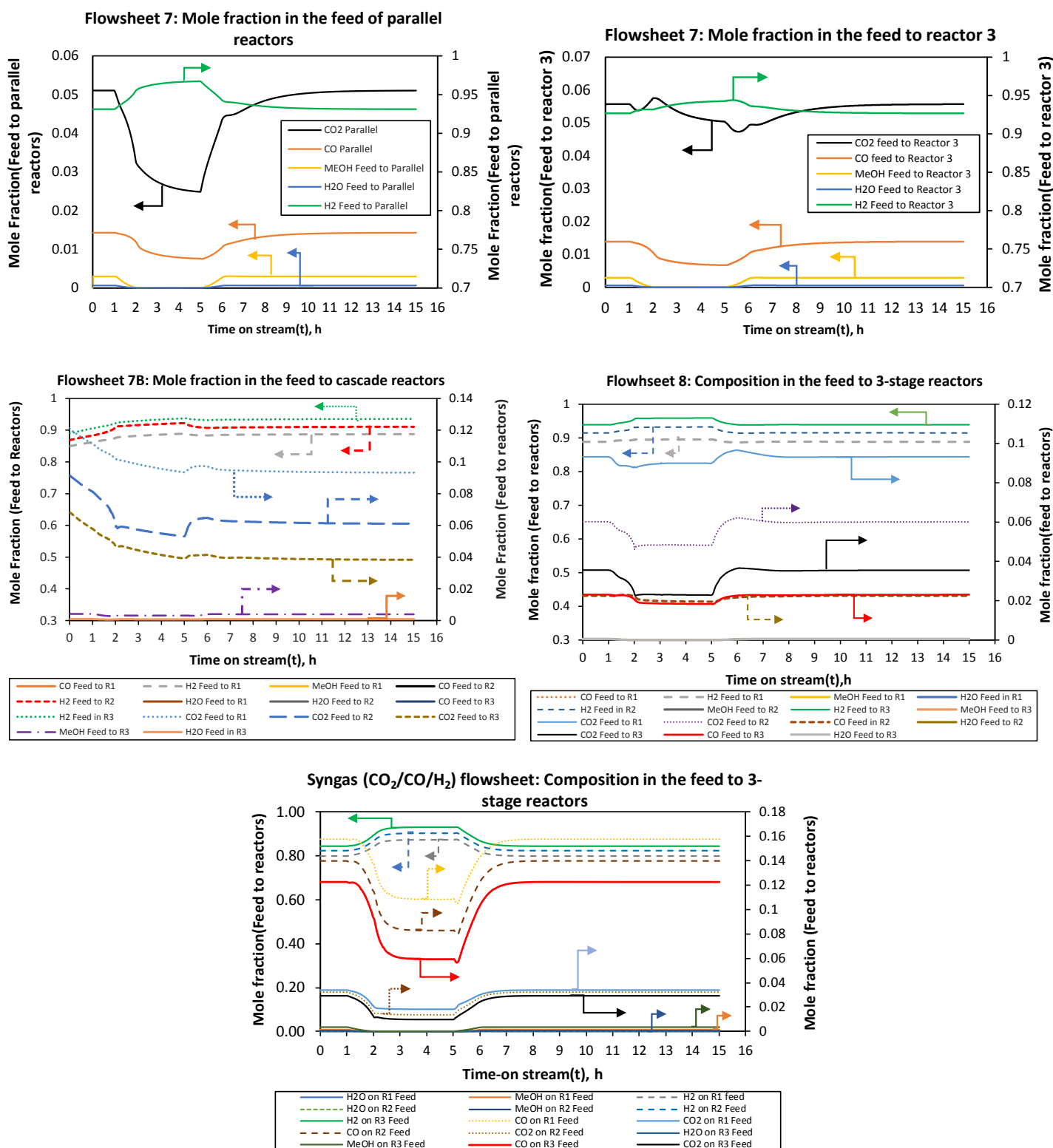


Figure 9: Shows the compositions of the feed streams to the reactors when the load was changed from full (100%) to half-load (50%).



720 However, the H<sub>2</sub> fraction in the reactor feed follow an opposite trend to load change. When load is reduced  
721 the H<sub>2</sub> content at all reactor inlet increases for all flowsheets. This is attributed to the fact that much of CO<sub>2</sub>  
722 gets converted during the load change such that, hydrogen is present in excess due to the recycle. High  
723 hydrogen content is seen in the last stage reactor. This is an interesting finding that hydrogen is in excess  
724 in the feed of the load flexible reactor during part-load. There is a slightly decreasing trend in the CO<sub>2</sub>,  
725 methanol, H<sub>2</sub>O and CO composition for Reactor 3 in flowsheet 7 and 7B, while flowsheet 8 shows a  
726 relatively similar decrease as with other reactors.

727 This shows that in flowsheet 8 the concentration inertia is eliminated across the process which is required  
728 to ensure flexible operation. It takes longer hours for the composition to achieve steady state, at-least for  
729 flowsheet 7 compared to flowsheet 8 and syngas-based flowsheet, as the load change, more especially for  
730 the last stage reactor in flowsheet 7. For flowsheet 8 and syngas-based flowsheet, the compositions need  
731 fewer hours to return to normal steady state after the disturbance. The parallel-series configuration  
732 (flowsheet 7) had pronounced overshoots and undershoots in the H<sub>2</sub> and CO<sub>2</sub> compositions.

### 733 **3.3.3 Heat exchanger and compressor duties**

734 Following the analysis of the Figure 10, the duties of the heat exchanger and the power of the compressors  
735 follow almost the same linear trend as the load change for all configurations. Considering the compressors  
736 duty for flowsheet 7, 7B and 8, there seems to be a similar linear decrease trend in the power of the recycle  
737 compressor(s) with changes in load from full (100%) to part-load (50%). For example, the compressor  
738 power for flowsheet 8 decreased from 236 kW at full-load to 131 kW at part-load, which is almost a 55%  
739 decrease. This can also be attributed to the high conversion at part-load (see Figure 12 for trend on  
740 conversion). On the other hand, for all the coolers in the considered systems, there is an increase in the  
741 cooling duties. This trend is similar to what Cui et al. observed and attributed to the quality of heat in the  
742 exit streams from the reactors, i.e., low grade heat of reactor effluent streams demands more cooling duty  
743 at part-load.<sup>57</sup> This is indeed the main energy loss for the methanol synthesis as has been discussed by other  
744 authors.<sup>57</sup> However, the impact of effective heat integration (that doesn't constraint flexibility but  
745 maximises the economics of the process) must be studied. It is expected that this may reduce the cooling  
746 requirements/demands for the methanol synthesis section. Again, the thermal inertia for the considered  
747 designs seems to be negligible. However, this remains to be confirmed. The heat exchanger duties are high  
748 for parallel-series flowsheet 7 compared to the series-series configuration and the lowest exchanger duties  
749 are found in the syngas-based configuration, more especially for the heaters. For all configurations no  
750 unfeasible heat exchanger duties (e.g., negative duties for the reactor preheaters) were observed.

751



752

753

754

755

756

757

758

759

760

761

762

763

764

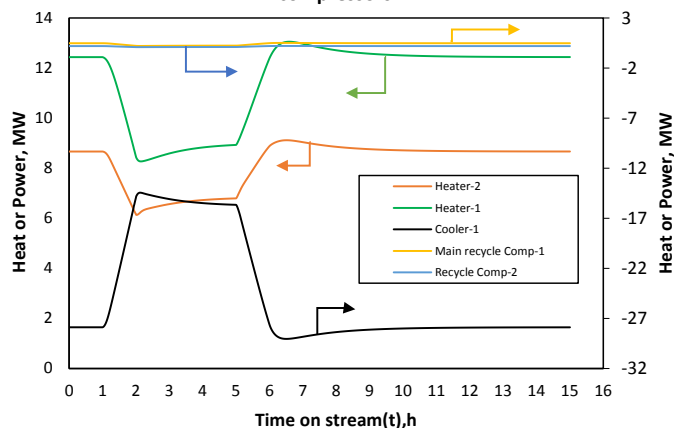
765

766

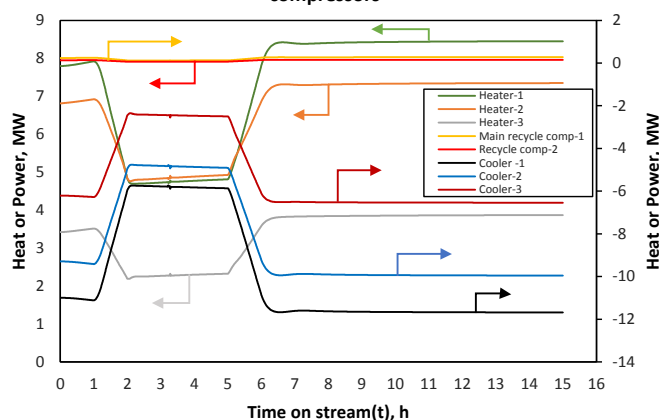
767

768

Flowsheet 7: duties for heat exchangers and power to the compressors



Flowsheet 7B: duties for heat exchangers and power for compressors



Flowsheet 8: duties for heat exchangers and power for the Compressor

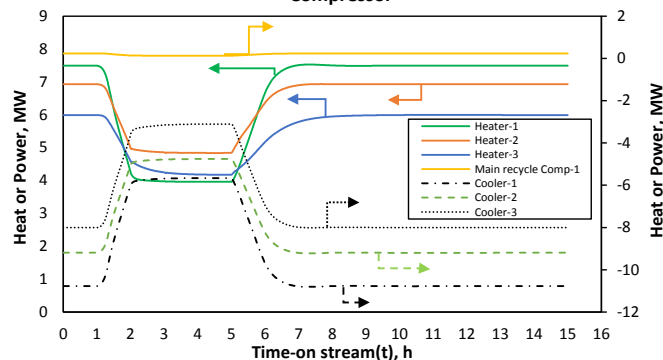
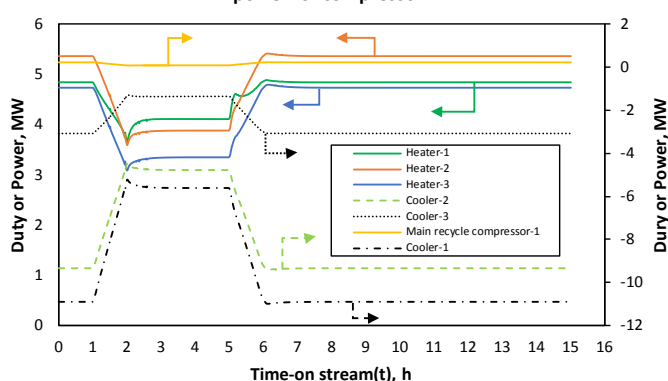
Syngas (CO/CO<sub>2</sub>/H<sub>2</sub>) flowsheet: duties for heat exchangers and power for compressor

Figure 10: Shows the heat duties and power of the compressors to the reactors when the load was changed from full (100%) to half-load (50%).

770

### 771 3.3.4 Load dependent energy efficiency

772 To assess the load dependency of the energy efficiency of the three methanol synthesis configurations, a  
 773 case without heat integration (no feed effluent heat exchange (FEHE) was simulated) while a case with  
 774 minimum reactor outlet-feed heat integration (HI) (via hypothetically FEHE) was assumed. The trend  
 775 depicted in Figure 11 shows a more pronounced decrease in energy efficiency with a decrease in the load  
 776 for all the flowsheets when the heat integration via feed effluent (without FEHE) is not considered. For  
 777 flowsheet 7 and 8, when the heat required to raise the temperature of the feed stream(s) to the reactor(s)  
 778 feed was set to zero (assuming there could be heat integration using FEHE), the energy efficiency shows a  
 779 very small variation from the full-load to all load levels (maximum, intermediate and minimum).





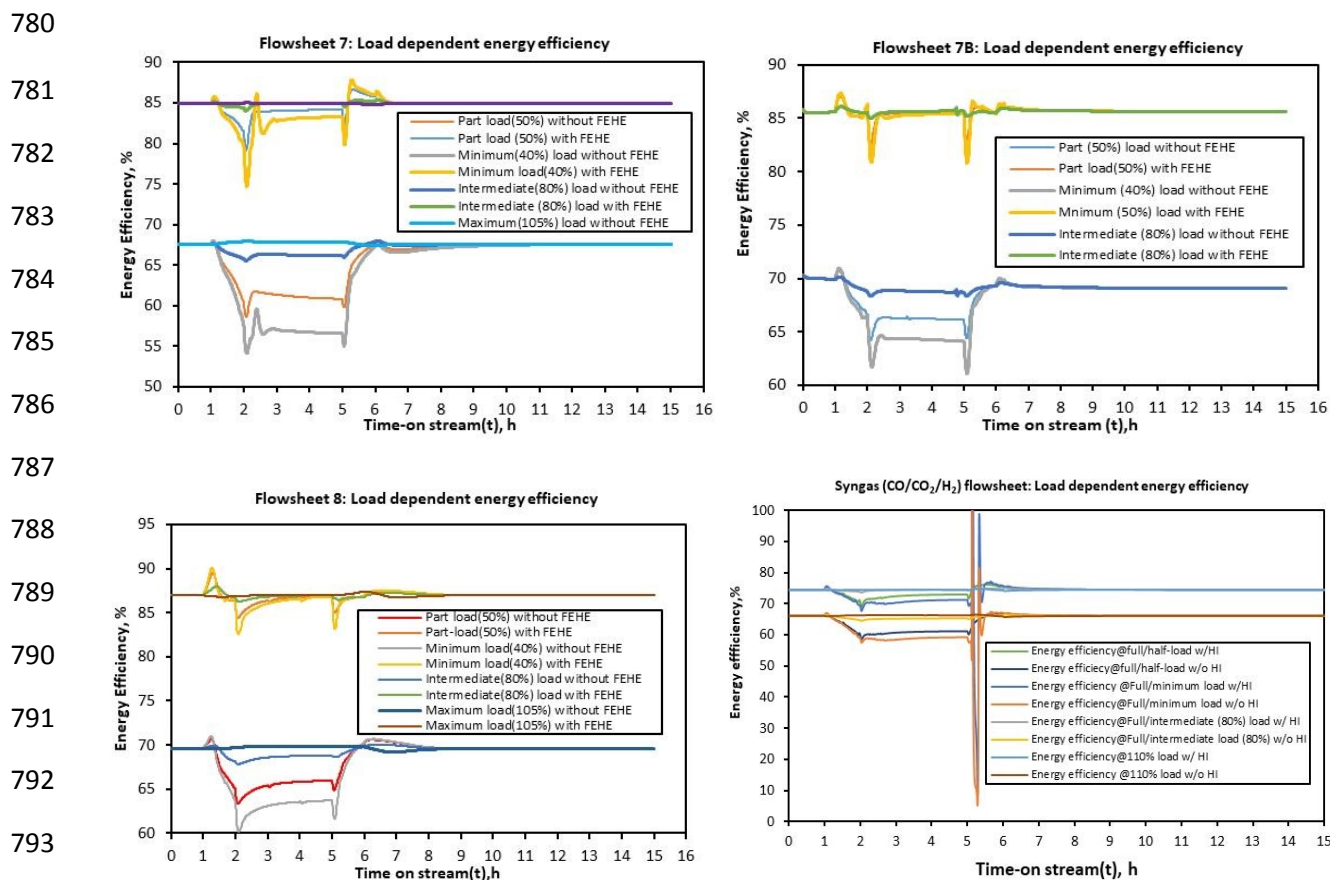


Figure 11: Shows the energy efficiency of the three configurations when the load was changed from full (105%) to half-load (50%), intermediate load (80%), and minimum load (40%). The ramp rate was kept constant at 60% load per hour.

For flowsheet 7B and 8, the energy efficiency is almost stable at steady state/full load energy efficiency when this minimum heat integration is considered. Although this heat integration is necessary to improve the energy efficiency, in real system it may induce the thermal oscillations due to tight coupling with the reactor. The assumption of a perfect (hypothetical) FEHE per reactor stage shows that enhancement of thermal dynamics is expected to improve the energy efficiency of the PtMeOH system. This will be more necessary and advantageous for the coupled methanol synthesis and upstream (electrolysis) at higher ramping rates since it is expected that the energy efficiency of the electrolysis will increase at low load and hence potentially increasing the overall energy efficiency of the coupled system.

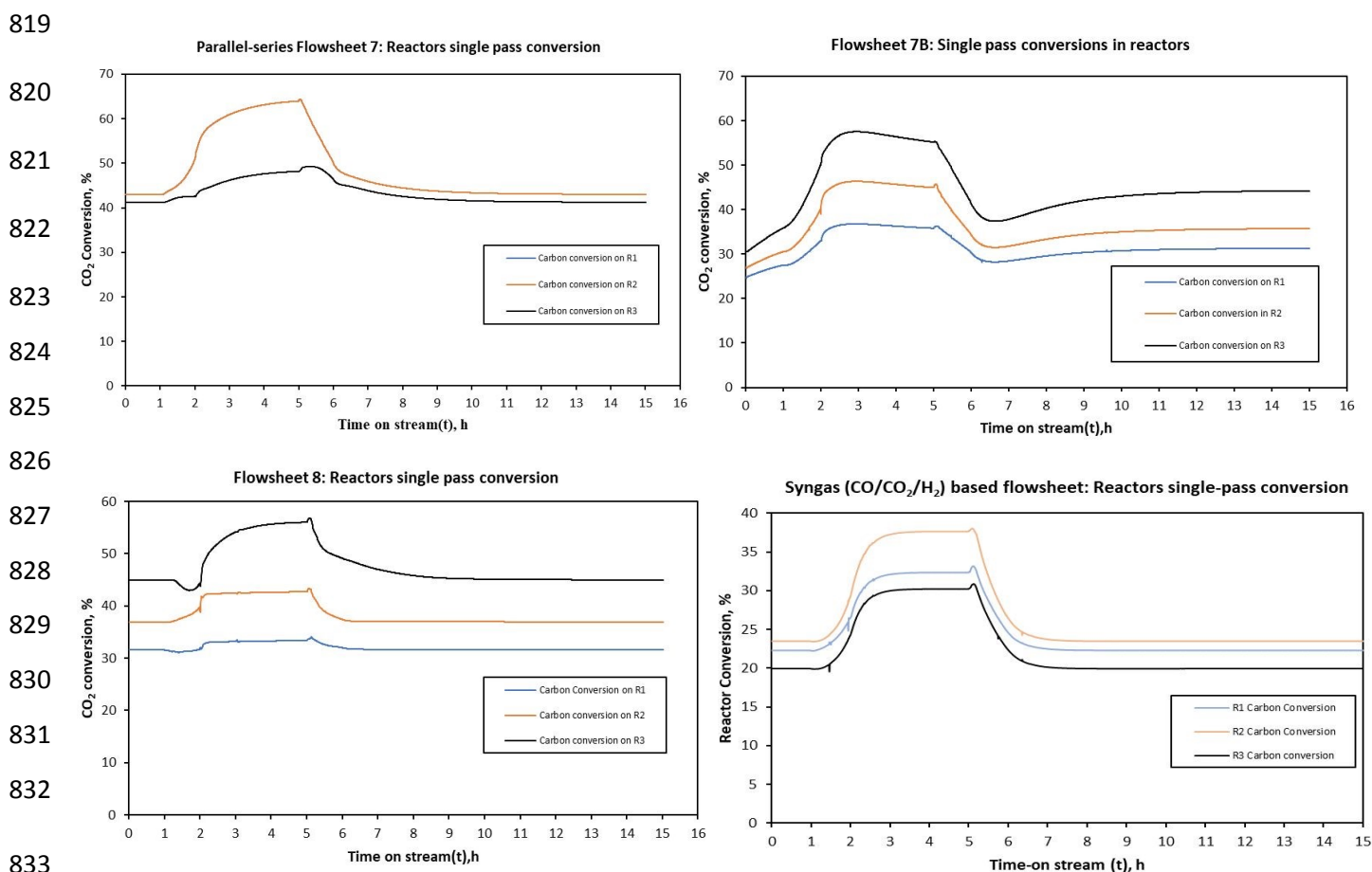
The findings on energy efficiency trend for flowsheets 7 and 8 are similar to the recent finding that for a direct methanol synthesis reactor, dynamic modelling studies suggest that for part-load production capacity the energy efficiency does not decrease significantly as also deduced by Cui et al.<sup>66</sup> The energy efficiency of the methanol synthesis system in flowsheet 8 is higher than the other flowsheets. This effect is however



809 dampened by the electrolysis and distillation units when the overall integrated steady state simulation was  
 810 considered in Figure 6 but it is expected to be more pronounced when effective heat integration is  
 811 considered. For the syngas-based route, the load dependent energy efficiency is found to be lower than the  
 812 other CO<sub>2</sub> hydrogenation systems, more especially when compared to flowsheet 8. The energy efficiency  
 813 fluctuates significantly with decrease in the load. At loads above the nominal, the energy efficiency doesn't  
 814 change significantly.

### 815 3.3.5 Single pass conversion

816 Conversion changes with load change. As illustrated in Figure 12, at part-load, the conversion is higher  
 817 than the conversion at full-load for all the configurations. This is expected as the reduction in flowrate  
 818 increases the residence time inside the reactor(s) and hence a positive step change in conversion result.



834 Figure 12: Shows the single pass reactor conversion for the three system configurations when the load was changed from full (105%) to half-load (50%).

835 The increase is slightly higher for parallel-series configuration in the parallel reactors (R1 and R2) due to  
 836 their capacity and the fact that each feed to these reactors is further decreased, i.e., split by 50%, and thus

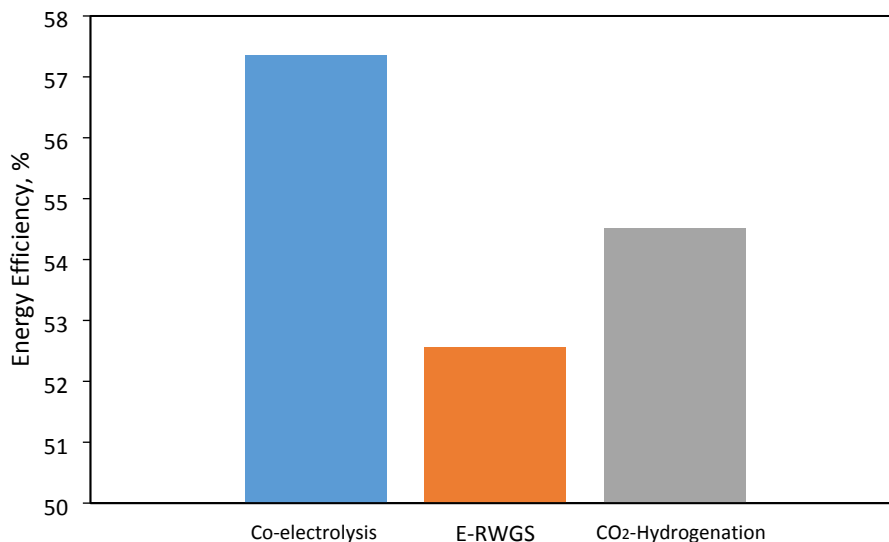


837 further rendering these reactors to operate at higher residence time than R3 and in contrast to R1, R2 and  
838 R3 of both configuration 7B, 8 and syngas-based flowsheet. For CO<sub>2</sub> hydrogenation-based flowsheet 7B  
839 and 8, conversion increases from first stage to last stage, with the last reactor stage having the highest single  
840 pass conversion compared to other reactors. However, the trend is opposite for the syngas-based reactor  
841 system. The second stage reactor has the highest conversion followed by the first stage and the last stage  
842 reactor.

### 843 **3.4. Comparison of CO-rich route based on e-RWGS and Co-electrolysis-based process to** 844 **the optimal CO<sub>2</sub> rich PtMeOH route.**

845 Production of CO-rich syngas can be done by either using a RWGS reactor or SOEC via co-electrolysis.  
846 Co-electrolysis offers a resource-saving and regenerative alternative to conventional syngas production.<sup>74-</sup>  
847 <sup>75</sup> The syngas delivered by co-electrolysis can be easily varied by changing the ratio of CO<sub>2</sub>/H<sub>2</sub>O and it is  
848 in the range (H<sub>2</sub>: CO at 1:1 to 3:1) desired for methanol synthesis. For fair comparison, the syngas feed  
849 coming from the electrolysis and e-RWGS was adjusted to 25.4/5.0/69.2% of CO/CO<sub>2</sub>/H<sub>2</sub> with 0.4% H<sub>2</sub>O  
850 to ensure similar methanol production rate as the CO<sub>2</sub> based process while maintaining the syngas ratio of  
851 2.1. Co-electrolysis is currently investigated in the current second phase of the Kopernikus project “P2X”  
852 at the Energy Lab 2.0 at the Karlsruhe Institute of Technology (KIT).<sup>74</sup> Herein the energy efficiency of the  
853 co-electrolysis is compared to the optimal direct PtMeOH process and the process with e-RWGS. Recently,  
854 Haldor Topsoe has highlighted its interest in developing a renewable energy electrified reverse water gas  
855 shift reactor (e-RWGS).<sup>76-77</sup> The utilization of an e-RWGS reactor in methanol synthesis follows the  
856 CAMERE process relying on fire heated RWGS reactors.<sup>76</sup> Basini et al. evaluated the potential of this step  
857 but never compared it to other trending technologies such as co-electrolysis and CO<sub>2</sub>-based PtMeOH overall  
858 processes under similar basis.<sup>76</sup> This section will discuss this comparison as it was modelled in this work.  
859 The SOEC-based co-electrolysis, steam electrolysis with and without e-RWGS are compared.





860  
861 Figure 13: Energy efficiency comparison of co-electrolysis, e-RWGS, and CO<sub>2</sub> based power to methanol  
862 process.

863 Following from Figure 13, the co-electrolysis-based process has the highest energy efficiency followed by  
864 the SOEC steam electrolysis-based CO<sub>2</sub>-hydrogenation and lastly the e-RWGS process. This is because  
865 the syngas produced from co-electrolysis in the SOEC has the higher heating value and the SOEC uses less  
866 heat under co-electrolysis compared to the steam electrolysis despite the co-electrolysis having higher  
867 electricity consumption.<sup>50</sup>

868 However, following from previous analysis, co-electrolysis may be flexible in terms of feed stock but for  
869 regions with largely fluctuating electricity up to very low loads, steam electrolysis-based methanol is  
870 recommended than the co-electrolysis-based process due to higher flexibility range of the CO<sub>2</sub>  
871 hydrogenation-based methanol process and the low power requirements for the SOEC steam electrolysis  
872 compared to SOEC-based on co-electrolysis mode as discussed in section 3.1. However, other factors may  
873 come into play such as the site-specific conditions, CO<sub>2</sub> emission reduction targets of the process and  
874 desired production rates.<sup>78-79</sup>

#### 875 4. CONCLUSIONS

876 This work has compared twelve different SOEC-based power-to-methanol process configurations. The  
877 performance of the SOEC under steam- and co-electrolysis-based operation were first modelled and  
878 compared. The results shows that steam electrolysis uses less power than the co-electrolysis. However, the  
879 co-electrolysis based SOEC leads to the highest energy efficiency. Following from this, different adiabatic  
880 reactor configurations based on CO<sub>2</sub> hydrogenation were compared. Among these configurations, parallel-



881 parallel, parallel-series and series-series based configurations were integrated with the SOEC unit operating  
882 under steam electrolysis and compared considering the overall energy efficiency, conversion, production  
883 rate, and single pass conversion profiles. Three candidate process flowsheet featuring parallel-series and  
884 series-series based configuration were selected for further comparison. The selected parallel-series  
885 configurations (flowsheet 7) feature three reactors in which the first two are in parallel and in series with  
886 the third adiabatic reactor.

887 The selected promising series-series configuration (flowsheet 7B and 8) features three reactors in series  
888 with intermediate cooling and separation. Thereafter the sensitivity-based analysis or optimisation and heat  
889 integration are performed on the most promising flowsheets. The series-series configuration showed low  
890 utility requirements upon optimisation of the heat exchanger network. To further assess the potential of  
891 these configurations, dynamic simulation was performed using Aspen Dynamics to assess their flexibility  
892 in terms of load change and considering parameters such as load change flexibility range, time to steady  
893 state, composition changes, heat duty, power of the main units, load dependent energy efficiency, and single  
894 pass reactor conversion profile. The dynamic simulation also featured the comparison of CO<sub>2</sub>  
895 hydrogenation-based, and syngas (derived from co-electrolysis) based flowsheets. Time to reach steady  
896 state was shorter for parallel-series configuration compared to series-series configuration but the allowable  
897 load flexibility range (40-105%) is similar for all the three CO<sub>2</sub>-based configurations. This indicates the  
898 potential to reduce the size of the intermediate product storage (e.g., H<sub>2</sub> storage) and allowing more flexible  
899 direct coupling of the electrolysis and methanol synthesis sections. The syngas-based flowsheet, although  
900 similar in architecture to the CO<sub>2</sub> hydrogenation-based flowsheet 8, cannot be ramped down to below 45%  
901 of the nominal load. Flowsheet 8 had the highest load dependent energy efficiency and reduced instabilities  
902 (undershoots and overshoots). Conversion increases with reduced load for all flowsheets. Overall,  
903 considering all factors, the series-based configuration with three adiabatic reactors in series is the most  
904 promising configuration. Multistage reactors offer the opportunity to promote flexibility by reducing the  
905 reactor overdesign, and allow for operating one reactor per time based on the available power supply and  
906 allowable idle period/downtime as may be set to prevent reactor damages and potential catalyst  
907 deactivation.

## 908 5. FUTURE WORK

909 Future work must conduct techno-economics of the flowsheets to better discriminate among the three  
910 candidate flowsheets for CO<sub>2</sub> hydrogenation. Furthermore, when the stoichiometric SOEC steam  
911 electrolysis-based integrated methanol synthesis is compared to co-electrolysis-based and to the e-RWGS-  
912 based configurations, the e-RWGS showed worse performance in terms of energy efficiency.



913 Although it has been demonstrated in this work that reactor configuration plays an important role in the  
914 performance of the dynamic power-to-methanol process, especially when the high efficiency electrolyser  
915 technology is used, more work is required to understand the dynamic operation strategies such as cold start-  
916 up, warm-standby, hot-standby and shutdown, and their effect on degradation and profitability of the  
917 process. For example, in the case of power-to-methanol operated with variable electricity, the reactor may  
918 need to be kept at stand-by mode to avoid condensation for example by recirculating the feed by means of  
919 bypassing the separator and shutting the purge thereby creating a batch system. Due to the enormous amount  
920 of energy required by the power-to-methanol via CO<sub>2</sub> hydrogenation, opportunities exist to further optimise  
921 the energy efficiency of the system with the intermediate product storage included. This must be assessed.

922 From the dynamic flexibility study conducted for the methanol synthesis section in this paper, it emanates  
923 that power to methanol will offer both flexibility and long-term energy storage in future markets. More  
924 data on hydrogen production are needed to further optimize the process. Future work should consider effects  
925 of perturbation of the feed conditions on the dynamics of the hot-spot temperature and methanol production  
926 from the low-cost adiabatic reactor as may be prevalent in the cases where variable power is used in power-  
927 to-methanol process. This includes variation of H<sub>2</sub>-to-CO<sub>2</sub> ratio. The H<sub>2</sub>-to-CO<sub>2</sub> ratio may be a major  
928 manipulable parameter in the case when renewable energy is used in power to methanol system. In this  
929 study, the CO<sub>2</sub> is assumed continuous and thus dynamic effects as well as the associated CO<sub>2</sub> storage are  
930 not considered. Future work should also consider the comparison of the heat integration potential when  
931 using water-cooled reactor which generates medium pressure steam against the adiabatic reactor in the case  
932 of power-to-methanol, in particular the steam utilization effect of coupling medium pressure steam to  
933 SOEC. This should also consider the thermal inertia in the catalyst and its effect on the process performance.

934 In addition, because of different loads, the time co-ordination of heat recovery between various heat sources  
935 and sinks must be assessed as well as its associated economics and energy efficiency. This study considered  
936 constant pressure drop in the reactor. It would be necessary to consider variation in the pressure drop and  
937 effect of modifying the reactor design, e.g., internals, on the optimization of the proposed load flexible  
938 design. Future work should also consider integrating stochastic forecasting market model to the flexible  
939 process for advantageous response to different electricity prices and methanol selling prices. This can also  
940 be coupled with methanol fuel cells. In this work, simplified models were used to study the best  
941 configuration with minimal complexity and thus future work must consider more detailed (e.g. 2D) models  
942 including improved kinetic models (formulated with dynamic experimental conditions as well non-  
943 negligible heat and mass transports) for better optimisation of the load flexible reactor configuration while  
944 considering the sample electricity variation cycle and its corresponding H<sub>2</sub> and CO<sub>2</sub> production from the  
945 coupled electrolysis and capture processes, respectively. Other intensification methods such as structured  
946 reactors/catalysts must also be investigated and compared. It would also be interesting to understand the





947 significance of methanol reactor dynamics on the overall integrated efficiency of the PtMeOH process and  
948 quantify the benefit in terms of the overall plant availability.

## 949 **DECLARATION OF COMPETING INTEREST**

950 The authors declare that they have no known competing financial interests or personal relationships that  
951 could have appeared to influence the work reported on this paper.

## 952 **ACKNOWLEDGEMENTS**

953 This work was supported by the South African Department of Science and Innovation (DSI) for research  
954 activities under the HySA Infrastructure Centre of Competence (KP5 program, Project No. CNMH17X)  
955 and by the Council for Scientific and Industrial Research (CSIR) (Project Nos: C1GEN25, C8GOH26).

## 956 **SUPPLEMENTARY MATERIAL**

957 The Supporting Information is available free of charge on the attached supplementary material document.

### **Nomenclature**

Symbol	Meaning (Unit)
AWE	Alkaline-water based electrolyser (–)
$b_i$	Logarithmic Arrhenius constants(–)
e-RWGS	Electrified Reverse Water Gas Shift Reactor
$\Delta G$	Gibbs free energy ( $\text{J mol}^{-1}$ )
$\Delta H_r$	Heat of reaction ( $\text{kJ mol}^{-1}$ )
COR	Carbon oxide ratio (–)
GHSV <sub>0</sub>	Gas hourly space velocity at nominal standard conditions ( $\text{h}^{-1}$ )
GHSV	Gas hourly space velocity ( $\text{NL.h}^{-1}.\text{gcat}^{-1}$ )
HEN	Heat Exhnager Network
LCOM	Levelised cost of methanol ( $\$/\text{tMEOH}$ )
$k_j$	Reaction rate constant (–)
$K_i$	Adsorption constant (–)
$M_{w_i}$	Molecular weight ( $\text{kg mol}^{-1}$ )
$m_c$	Mass of the catalyst (kg)
$m_i$	Mass of component (kg)
PteMeOH	Power to methanol
R	Ideal gas constant ( $\text{J mol}^{-1}\text{K}^{-1}$ )



RKSMHV2	Redlich-Kwong Soave with Modified Huron-Vidal mixing rules
SN	Stoichiometric number (–)
T	Temperature (K)
SOEC	Solid oxide electrolyser (–)
$\varepsilon$	Fixed bed porosity (–)
$\rho_{cat}$	Catalyst density (kg m <sup>-3</sup> )

958

959

960 **REFERENCES**

- 961 1. Salmon N, Bañares-Alcántara R. Green ammonia as a spatial energy vector: a review. *Sustainable*  
962 *Energy & Fuels*. 2021.
- 963 2. Giannoulidis S, Venkataraman V, Woudstra T, Aravind PV. Methanol based Solid Oxide  
964 Reversible energy storage system–Does it make sense thermodynamically?. *Applied Energy*. 2020  
965 Nov 15;278:115623.
- 966 3. Hank, C., Sternberg, A., Köppel, N., Holst, M., Smolinka, T., Schaadt, A., Hebling, C. and  
967 Henning, H.M., 2020. Energy efficiency and economic assessment of imported energy carriers  
968 based on renewable electricity. *Sustainable Energy & Fuels*, 4(5), pp.2256-2273.
- 969 4. Moiola, E., Mutschler, R. and Züttel, A., 2019. Renewable energy storage via CO<sub>2</sub> and H<sub>2</sub>  
970 conversion to methane and methanol: Assessment for small scale applications. *Renewable and*  
971 *Sustainable Energy Reviews*, 107, pp.497-506.
- 972 5. Chein RY, Chen WH, Ong HC, Show PL, Singh Y. Analysis of methanol synthesis using CO<sub>2</sub>  
973 hydrogenation and syngas produced from biogas-based reforming processes. *Chemical*  
974 *Engineering Journal*. 2021 Jun 15:130835.
- 975 6. Zheng Y, You S, Li X, Bindner HW, Münster M. Data-driven robust optimization for optimal  
976 scheduling of power to methanol. *Energy Conversion and Management*. 2022 Mar 15;256:115338.
- 977 7. González-Garay A, Frei MS, Al-Qahtani A, Mondelli C, Guillén-Gosálbez G, Pérez-Ramírez J.  
978 Plant-to-planet analysis of CO<sub>2</sub>-based methanol processes. *Energy & Environmental Science*.  
979 2019;12(12):3425-36.
- 980 8. Vázquez D, Guillén-Gosálbez G. Process design within planetary boundaries: Application to CO<sub>2</sub>  
981 based methanol production. *Chemical Engineering Science*. 2021 Jun 21:116891.
- 982 9. Luyben WL. Design and control of a methanol reactor/column process. *Industrial & engineering*  
983 *chemistry research*. 2010 Jul 7;49(13):6150-63.



- 984 10. Hankin A, Shah N. Process exploration and assessment for the production of methanol and  
985 dimethyl ether from carbon dioxide and water. *Sustainable Energy & Fuels*. 2017;1(7):1541-56.
- 986 11. Gogate MR. Methanol synthesis revisited: reaction mechanisms in CO/CO<sub>2</sub> hydrogenation over  
987 Cu/ZnO and DFT analysis. *Petroleum Science and Technology*. 2019 Mar 4;37(5):603-10.
- 988 12. Bowker M. Methanol synthesis from CO<sub>2</sub> hydrogenation. *ChemCatChem*. 2019 Sep 5;11(17):4238.
- 989 13. Stefansson B. Power and CO<sub>2</sub> emissions to methanol. In *Presentation, 2015 European methanol*  
990 *policy forum 2015 Oct*.
- 991 14. Lee HW, Kim K, An J, Na J, Kim H, Lee H, Lee U. Toward the practical application of direct CO<sub>2</sub>  
992 hydrogenation technology for methanol production. *International Journal of Energy Research*.
- 993 15. Jiang X, Nie X, Guo X, Song C, Chen JG. Recent Advances in Carbon Dioxide Hydrogenation to  
994 Methanol via Heterogeneous Catalysis. *Chemical Reviews*. 2020 Feb 12.
- 995 16. Ruland H, Song H, Laudenschleger D, Stürmer S, Schmidt S, He J, Kähler K, Muhler M, Schlögl  
996 R. CO<sub>2</sub> hydrogenation with Cu/ZnO/Al<sub>2</sub>O<sub>3</sub>: A benchmark study. *ChemCatChem*. 2020 Apr 21.
- 997 17. Bos MJ, Kersten SR, Brillman DW. Wind power to methanol: Renewable methanol production  
998 using electricity, electrolysis of water and CO<sub>2</sub> air capture. *Applied Energy*. 2020 Apr  
999 15;264:114672.
- 1000 18. Al-Kalbani H, Xuan J, García S, Wang H. Comparative energetic assessment of methanol  
1001 production from CO<sub>2</sub>: Chemical versus electrochemical process. *Applied energy*. 2016 Mar  
1002 1;165:1-3.
- 1003 19. Pérez-Fortes M, Schöneberger JC, Boulamanti A, Tzimas E. Methanol synthesis using captured  
1004 CO<sub>2</sub> as raw material: Techno-economic and environmental assessment. *Applied Energy*. 2016 Jan  
1005 1;161:718-32.
- 1006 20. Zhang H, Wang L, Pérez-Fortes M, Maréchal F, Desideri U. Techno-economic optimization of  
1007 biomass-to-methanol with solid-oxide electrolyzer. *Applied Energy*. 2020 Jan 15;258:114071.
- 1008 21. Rivera-Tinoco R, Farran M, Bouallou C, Auprêtre F, Valentin S, Millet P, Ngameni JR.  
1009 Investigation of power-to-methanol processes coupling electrolytic hydrogen production and  
1010 catalytic CO<sub>2</sub> reduction. *International Journal of Hydrogen Energy*. 2016 Mar 2;41(8):4546-59.
- 1011 22. Zhang H, Wang L, Maréchal F, Desideri U. Techno-economic optimization of CO<sub>2</sub>-to-methanol  
1012 with solid-oxide electrolyzer. *Energies*. 2019 Jan;12(19):3742.
- 1013 23. Alsuhaibani AS, Afzal S, Challiwala M, Elbashir NO, El-Halwagi MM. The impact of the  
1014 development of catalyst and reaction system of the methanol synthesis stage on the overall  
1015 profitability of the entire plant: A techno-economic study. *Catalysis Today*. 2020 Mar 1;343:191-  
1016 8.



- 1017 24. GhasemiKafrudi E, Samiee L, Pour ZM, Rostami T. Optimization of methanol production process  
1018 from carbon dioxide hydrogenation in order to reduce recycle flow and energy consumption.  
1019 Journal of Cleaner Production. 2022 Sep 23:134184.
- 1020 25. Zondervan E, editor. Process Systems Engineering: For a Smooth Energy Transition. Walter de  
1021 Gruyter GmbH & Co KG; 2022 Oct 3.
- 1022 26. Voß JM, Duan T, Geitner C, Schluter S, Schulzke T. Operating behavior of a demonstration plant  
1023 for methanol synthesis, Chemie Ingenieur Technik. 2022 Oct; 94(10): 1489-500.
- 1024 27. Rodriguez Vallejo D. Promoting sustainability in chemical process design using process modelling,  
1025 environmental assessment and decision making (Doctoral dissertation, Imperial College London).
- 1026 28. Chiou HH, Lee CJ, Wen BS, Lin JX, Chen CL, Yu BY. Evaluation of alternative processes of  
1027 methanol production from CO<sub>2</sub>: Design, optimization, control, techno-economic, and  
1028 environmental analysis. Fuel. 2023 Jul 1;343:127856.
- 1029 29. Zhou H, Wang J, Meng W, Wang K, Li G, Yang Y, Fan Z, Wang D, Ji D. Comparative investigation  
1030 of CO<sub>2</sub>-to-methanol process using different CO<sub>2</sub> capture technologies. Fuel. 2023 Apr  
1031 15;338:127359.
- 1032 30. Bruns B, Herrmann F, Polyakova M, Grünewald M, Riese J. A systematic approach to define  
1033 flexibility in chemical engineering. Journal of Advanced Manufacturing and Processing. 2020  
1034 Oct;2(4):e10063.
- 1035 31. Chen C, Yang A. Power-to-methanol: The role of process flexibility in the integration of variable  
1036 renewable energy into chemical production. Energy Conversion and Management. 2021 Jan  
1037 15;228:113673.
- 1038 32. Mucci S, Mitsos A, Bongartz D. Power-to-X processes based on PEM water electrolyzers: A review  
1039 of process integration and flexible operation. Computers & Chemical Engineering. 2023 Apr  
1040 14:108260.
- 1041 33. Qi M, Vo DN, Yu H, Shu CM, Cui C, Liu Y, Park J, Moon I. Strategies for flexible operation of  
1042 power-to-X processes coupled with renewables. Renewable and Sustainable Energy Reviews. 2023  
1043 Jun 1;179:113282.
- 1044 34. Bruns B, Grünewald M, Riese J. Optimal design for flexible operation with multiple fluctuating  
1045 input parameters. In Computer Aided Chemical Engineering 2022 Jan 1 (Vol. 51, pp. 859-864).  
1046 Elsevier.
- 1047 35. Qiu Y, Zhou B, Zang T, Zhou Y, Qi R, Lin J. Extended Load Flexibility of Industrial P2H Plants:  
1048 A Process Constraint-Aware Scheduling Approach. arXiv preprint arXiv:2203.02991. 2022 Mar 6.



- 1049 36. Lange H, Klose A, Lippmann W, Urbas L. Technical evaluation of the flexibility of water  
1050 electrolysis systems to increase energy flexibility: A review. *International Journal of Hydrogen*  
1051 *Energy*. 2023 Jan 31.
- 1052 37. Li G, Gou Y, Ren R, Xu C, Qiao J, Sun W, Wang Z, Sun K. Realizing high-temperature steam  
1053 electrolysis on tubular solid oxide electrolysis cells sufficing multiple and rapid start-up. *Ceramics*  
1054 *International*. 2023 May 1;49(9):14101-8.
- 1055 38. Zimmermann RT, Bremer J, Sundmacher K. Load-flexible fixed-bed reactors by multi-period  
1056 design optimization. *Chemical Engineering Journal*. 2021 Jun 10:130771.
- 1057 39. Salmon N, Bañares-Alcántara R. Impact of process flexibility and imperfect forecasting on the  
1058 operation and design of Haber–Bosch green ammonia. *RSC Sustainability*. 2023.
- 1059 40. Grossmann IE, Morari M. Operability, resiliency, and flexibility: Process design objectives for a  
1060 changing world.
- 1061 41. Rinaldi R, Visconti CG. Flexible operations of a multi-tubular reactor for methanol synthesis from  
1062 biogas exploiting green hydrogen. *Chemical Engineering Science*. 2023 May 15;272:118611.
- 1063 42. Svitnič T, Sundmacher K. Renewable methanol production: Optimization-based design, scheduling  
1064 and waste-heat utilization with the FluxMax approach. *Applied Energy*. 2022 Nov 15;326:120017.
- 1065 43. Siemens, 2024. Retrieved from: [https://www.siemens-energy.com/global/en/home/products-](https://www.siemens-energy.com/global/en/home/products-services/product-offerings/hydrogen-solutions.html)  
1066 [services/product-offerings/hydrogen-solutions.html](https://www.siemens-energy.com/global/en/home/products-services/product-offerings/hydrogen-solutions.html)
- 1067 44. Copenhagen Infrastructure Partners (CIP), 2021. Retrieved from:  
1068 <https://renewablesnow.com/news/cip-plans-power-to-x-plant-to-produce-green-methanol-764426/>
- 1069 45. Sánchez-Luján J, Molina-García Á, López-Cascales JJ. Optimal integration modeling of Co–  
1070 Electrolysis in a power-to-liquid industrial process. *International Journal of Hydrogen Energy*.  
1071 2024 Jan 2;52:1202-19.
- 1072 46. Samimi F, Feilizadeh M, Najibi SB, Arjmand M, Rahimpour MR. Carbon dioxide utilization in  
1073 methanol synthesis plant: process modeling. *Chemical Product and Process Modeling*. 2020 Nov  
1074 2;1(ahead-of-print).
- 1075 47. Rahimpour MR, Ghader S, Baniadam M, Fathi Kalajahi J. Incorporation of flexibility in the design  
1076 of a methanol synthesis loop in the presence of catalyst deactivation. *Chemical Engineering &*  
1077 *Technology: Industrial Chemistry-Plant Equipment-Process Engineering-Biotechnology*. 2003 Jun  
1078 4;26(6):672-8.
- 1079 48. Léonard, G., Giulini, D. and Villarreal-Singer, D., 2016. Design and evaluation of a high-density  
1080 energy storage route with CO<sub>2</sub> re-use, water electrolysis and methanol synthesis. In *Computer*  
1081 *Aided Chemical Engineering* (Vol. 38, pp. 1797-1802). Elsevier.



- 1082 49. Kontogeorgis GM, Folas GK. The EoS/GE mixing rules for cubic equations of state.  
1083 Thermodynamic Models for Industrial Applications: From Classical and Advanced Mixing Rules  
1084 to Association Theories. John Wiley & Sons, Ltd, Chichester. 2010:159-93.
- 1085 50. Patcharavorachot Y, Chatrattanawet N, Arpornwichanop A, Saebea D. Comparative energy,  
1086 economic, and environmental analyses of power-to-gas systems integrating SOECs in steam-  
1087 electrolysis and co-electrolysis and methanation. Thermal Science and Engineering Progress. 2023  
1088 May 11:101873.
- 1089 51. Lonis, F. Design, modelling, evaluation and comparison of energy systems for the production and  
1090 use of renewable methanol using recycled CO<sub>2</sub>. PhD thesis. University of Cagliari, 2020
- 1091 52. Sunfire-Factsheet-HyLink-SOEC-20210303,  
1092 [https://www.sunfire.de/files/sunfire/images/content/Sunfire.de%20\(neu\)/Sunfire-Factsheet-  
1094 HyLink-SOEC-20210303.pdf](https://www.sunfire.de/files/sunfire/images/content/Sunfire.de%20(neu)/Sunfire-Factsheet-<br/>1093 HyLink-SOEC-20210303.pdf)
- 1095 53. Sunfire-Factsheet-SynLink-SOEC-20210303,  
1096 [https://www.sunfire.de/files/sunfire/images/content/Sunfire.de%20\(neu\)/Sunfire-Factsheet-  
1098 SynLink-SOEC-20210303.pdf](https://www.sunfire.de/files/sunfire/images/content/Sunfire.de%20(neu)/Sunfire-Factsheet-<br/>1097 SynLink-SOEC-20210303.pdf)
- 1099 54. Hansen JB, Christiansen N, Nielsen JU. Production of sustainable fuels by means of solid oxide  
1100 electrolysis. ECS Transactions. 2011 Apr 25;35(1):2941.
- 1101 55. Hossein Nami, Omid Babaie Rizvandi, Christodoulos Chatzichristodoulou, Peter Vang  
1102 Hendriksen, Henrik Lund Frandsen, Techno-economic analysis of current and emerging electrolysis  
1103 technologies for green hydrogen production, Energy Conversion and Management, Volume 269,  
1104 2022, 116162, ISSN 0196-8904, <https://doi.org/10.1016/j.enconman.2022.116162>.
- 1105 56. Wang, L., Chen, M., Küngas, R., Lin, T.E., Diethelm, S. and Maréchal, F., 2019. Power-to-fuels  
1106 via solid-oxide electrolyzer: Operating window and techno-economics. Renewable and Sustainable  
1107 Energy Reviews, 110, pp.174-187.
- 1108 57. Im-orb K, Visitdumrongkul N, Saebea D, Patcharavorachot Y, Arpornwichanop A. Flowsheet-  
1109 based model and exergy analysis of solid oxide electrolysis cells for clean hydrogen production.  
1110 Journal of Cleaner Production. 2018 Jan 1;170:1-3.
- 1111 58. Jamshidi S, Sedaghat MH, Amini A, Rahimpour MR. CFD simulation and sensitivity analysis of  
1112 an industrial packed bed methanol synthesis reactor. Chemical Engineering and Processing-Process  
1113 Intensification. 2023 Jan 1;183:109244.
- 1114 59. Lonis, F., Tola, V., Cascetta, M., Arena, S. and Cau, G., 2019, December. Performance evaluation  
1115 of an integrated energy system for the production and use of renewable methanol via water  
electrolysis and CO<sub>2</sub> hydrogenation. In AIP Conference Proceedings (Vol. 2191, No. 1, p. 020099).  
AIP Publishing LLC.





- 1116 60. Lonis, F., Tola, V. and Cau, G., 2019. Renewable methanol production and use through reversible  
1117 solid oxide cells and recycled CO<sub>2</sub> hydrogenation. *Fuel*, 246, pp.500-515.
- 1118 61. Kiss, A.A., Pragt, J.J., Vos, H.J., Bargeman, G. and De Groot, M.T., 2016. Novel efficient process  
1119 for methanol synthesis by CO<sub>2</sub> hydrogenation. *Chemical engineering journal*, 284, pp.260-269.
- 1120 62. Cui, X. and Kær, S.K., 2020. A comparative study on three reactor types for methanol synthesis  
1121 from syngas and CO<sub>2</sub>. *Chemical Engineering Journal*, p.124632.
- 1122 63. Bussche KV, Froment GF. A steady-state kinetic model for methanol synthesis and the water gas  
1123 shift reaction on a commercial Cu/ZnO/Al<sub>2</sub>O<sub>3</sub>Catalyst. *Journal of Catalysis*. 1996 Jun 1;161(1):1-  
1124 0.
- 1125 64. Van-Dal, É.S. and Bouallou, C., 2013. Design and simulation of a methanol production plant from  
1126 CO<sub>2</sub> hydrogenation. *Journal of Cleaner Production*, 57, pp.38-45.
- 1127 65. Mignard D, Pritchard C. On the use of electrolytic hydrogen from variable renewable energies for  
1128 the enhanced conversion of biomass to fuels. *Chemical engineering research and design*. 2008 May  
1129 1;86(5):473-87.
- 1130 66. Cui X, Kær SK, Nielsen MP. Energy analysis and surrogate modeling for the green methanol  
1131 production under dynamic operating conditions. *Fuel*. 2021 Sep.
- 1132 67. Nestler, F., Schütze, A.R., Ouda, M., Hadrich, M.J., Schaadt, A., Bajohr, S., Kolb, T., 2020.  
1133 Kinetic modelling of methanol synthesis over commercial catalysts: A critical assessment, *Chem.*  
1134 *Eng. J.* 394, 124881. <https://doi.org/10.1016/j.cej.2020.124881>.
- 1135 68. Slotboom, Y., Bos, M.J., Pieper, J., Vrieswijk, V., Likoazar, B., Kersten, S.R., Brilman, D.W., 2020  
1136 Critical assessment of steady-state kinetic models for the synthesis of methanol over an industrial  
1137 Cu/ZnO/Al<sub>2</sub>O<sub>3</sub> catalyst, *Chem. Eng. J.* 389, 124181. <https://doi.org/10.1016/j.cej.2020.124181>.
- 1138 69. de Oliveira Campos, B.L., Herrera Delgado, K., Pitter, S., Sauer, J., 2021b. Development of  
1139 consistent kinetic models derived from a microkinetic model of the methanol synthesis, *Ind. Eng.*  
1140 *Chem. Res.* 60 (42), 15074–15086. <https://doi/full/10.1021/acs.iecr.1c02952>.
- 1141 70. Kiss, A.A., Pragt, J.J., van Iersel, M.M., Bargeman, G. and de Groot, M.T., 2013. Continuous  
1142 process for the preparation of methanol by hydrogenation of carbon dioxide. WIPO Patent  
1143 2013144041.
- 1144 71. Szima S, Cormos CC. Improving methanol synthesis from carbon-free H<sub>2</sub> and captured CO<sub>2</sub>: a  
1145 techno-economic and environmental evaluation. *Journal of CO<sub>2</sub> Utilization*. 2018 Mar 1;24:555-  
1146 63.
- 1147 72. Parigi D, Giglio E, Soto A, Santarelli M. Power-to-fuels through carbon dioxide Re-Utilization and  
1148 high-temperature electrolysis: A technical and economical comparison between synthetic methanol  
1149 and methane. *Journal of Cleaner Production*. 2019 Jul 20;226:679-91.



- 1150 73. Bansode A, Urakawa A. Towards full one-pass conversion of carbon dioxide to methanol and  
1151 methanol-derived products. *Journal of Catalysis*. 2014 Jan 1;309:66-70.
- 1152 74. de Hair B, Fantz U, Hecimovic A, Schulz A, Navarrete Munoz A, Klumpp M. Trend report  
1153 technical chemistry 2021. *News from chemistry*. 2021 Jun; 69 (6): 52-9.
- 1154 75. Zhan Z, Kobsiriphat W, Wilson JR, Pillai M, Kim I, Barnett SA. Syngas production by  
1155 coelectrolysis of CO<sub>2</sub>/H<sub>2</sub>O: the basis for a renewable energy cycle. *Energy & Fuels*. 2009 Jun  
1156 18;23(6):3089-96.
- 1157 76. Basini LE, Furesi F, Baumgärtl M, Mondelli N, Pauletto G. CO<sub>2</sub> capture and utilization (CCU) by  
1158 integrating water electrolysis, electrified reverse water gas shift (E-RWGS) and methanol synthesis.  
1159 *Journal of Cleaner Production*. 2022 Dec 1;377:134280.
- 1160 77. Thor Wismann S, Larsen KE, Mølgaard Mortensen P. Electrical Reverse Shift: Sustainable CO<sub>2</sub>  
1161 Valorization for Industrial Scale. *Angewandte Chemie*. 2022 Feb 14;134(8):e202109696.
- 1162 78. Tsiklios C, Schneider S, Hermesmann M, Müller TE. Efficiency and Optimal Load Capacity of E-  
1163 Fuel-Based Energy Storage Systems. *Advances in Applied Energy*. 2023 Apr 23:100140.
- 1164 79. Ioannou I, D'Angelo SC, Galán-Martín Á, Pozo C, Pérez-Ramírez J, Guillén-Gosálbez G. Process  
1165 modelling and life cycle assessment coupled with experimental work to shape the future sustainable  
1166 production of chemicals and fuels. *Reaction Chemistry & Engineering*. 2021.



## Data Availability Statement

View Article Online  
DOI: 10.1039/D4YA00433G

The data that support the findings of this study are available from the corresponding author upon reasonable request.

